International Journal of Heat and Fluid Flow 29 (2008) 1699–1715

Contents lists available at ScienceDirect

International Journal of Heat and Fluid Flow

journal homepage: www.elsevier.com/locate/ijhff

Effect of axisymmetric forcing on the structure of a swirling turbulent jet ☆

Sergey V. Alekseenko [a,b], Vladimir M. Dulin [a], Yuriy S. Kozorezov [a,b], Dmitriy M. Markovich [a,b,*]

[a] Institute of Thermophysics, Siberian Branch of RAS, Lavrentyev Avenue 1, Novosibirsk 630090, Russia
[b] Novosibirsk State University, Pirogova Street, 2, Novosibirsk 630090, Russia

ARTICLE INFO

Article history:
Received 5 November 2007
Received in revised form 30 June 2008
Accepted 27 July 2008
Available online 26 September 2008

Keywords:
Swirling jets
Turbulent jets
Control
External forcing
Stereo PIV
Conditional sampling

ABSTRACT

With the aid of the Stereo PIV technique, the local structure of swirling free turbulent jets is investigated under the following flow conditions: the Reynolds number was equal to 8900, and the swirl number varied from 0 to 1.0. The effect on the jet flow structure of external periodical forcing, applied with an axisymmetric mode to the inlet velocity, was studied. Also investigated were the flow response to the forcing at two Strouhal numbers, $St = 0.52$ and 1.2, and with various forcing amplitudes. Additional measurements with application of the conditional sampling approach were performed in order to analyze spatio-temporal dynamics of the large-scale ring-like vortices, generated in the forced jet at a low swirl rate. The greatest effect of the forcing on the swirling jet structure was observed in the case of the high swirl rate ($S = 1.0$), which was previously considered to be largely insensitive to external forcing. The forcing at $St = 1.2$ with relatively high amplitude resulted in an abrupt change in the turbulent structure of the flow: an increase of total turbulent kinetic energy and strong anisotropy of its components took place.

1. Introduction

The imposition of swirl on jet flows is often used in a number of industrial devices, burners, propulsion systems such as jet engines. In combustion facilities, one peculiarity of strongly swirling jets is the presence of reverse flow near the nozzle, which provides reliable stabilization of the flame. In chemical reactors and mixing chambers, faster spreading of the swirling jets relative to the non-swirling ones plays an important role and leads to greater entrainment of the surrounding media. A number of swirling flows is also observed in nature (tornados, water spouts, etc.) which have to be carefully studied in order to forecast and prevent catastrophes.

At the same time, the turbulent structure of jet flow depends strongly on the conditions of the swirl superimposition. Depending on the swirl rate and the manner in which the swirl is applied, substantially different flow regimes can be observed: vortex rings for non-swirling and weakly swirling jets; helical waves with different wavenumbers for strongly swirling jets (e.g., Alekseenko et al., 1999). Finally, a vortex breakdown (VB) appears for sufficiently high swirl rates. The VB is known to have different states (Alekseenko et al., 2007a): spiral, bubble, or conical, where the last two can be either symmetric or asymmetric (e.g., Billant et al., 1998). The bases of swirling flows are described in detail in the work of Gupta et al. (1984), and an introduction to the theory of helical vortices appearing in swirl flows can be found in Alekseenko et al. (2007c). Detailed studies of different types of swirling jet flows were done in a number of experimental, numerical and theoretical works, considering different inflow geometries (Ribeiro and Whitelaw, 1980; Mehta et al., 1991; Panda and McLaughlin, 1994; Shtern and Hussain, 1996; Billant et al., 1998; Sun et al., 2002; Gallaire and Chomaz, 2003, 2004; Loiseleux and Chomaz, 2003; Ruith et al., 2003; Gallaire et al., 2004; Cala et al., 2005; Liang and Maxworthy, 2005; Duwig and Fuchs, 2007; Mourtazin and Cohen, 2007; etc.). Most of these works are devoted to the analysis of azimuthal instabilities and to the study of VB dynamics in swirling jets at comparatively small Reynolds numbers (up to 1000). Concerning swirling jets at high Reynolds numbers, significantly fewer works reporting comprehensive data on turbulence characteristics can be found in the literature (e.g., Cala et al., 2005; Alekseenko et al., 2007a). It has been reported by many authors that Kelvin–Helmholtz instability in the jet shear layer leading to vortex ring formation dominates non-swirling and weakly swirling jets. For a high enough swirl rate (before VB), the strong helical waves are most pronounced in the jet mixing layer. Further increase of the swirl rate results in VB. Strong helical waves were usually observed in the outer mixing layer of the jet, and single and/or double helixes were determined in the VB region (e.g., Billant et al., 1998; Loiseleux et al., 1998; Ruith et al., 2003; Liang and Maxworthy, 2005). However, among these results there are substantially different flow regimes and VB states, which depend strongly on the inflow velocity profiles. The strong influence of buoyancy effects on the VB shape was also shown in the recent paper by Mourtazin and Cohen (2007).

☆ This paper was originally presented at the International Symposium on Turbulence and Shear Flow Phenomena held in Munich on August 26-29, 2007, and later expanded, revised, and submitted; See Volume 29 No 3, June 2008

* Corresponding author. Address: Institute of Thermophysics, Siberian Branch of RAS, Lavrentyev Avenue 1, Novosibirsk 630090, Russia. Tel.: +7 383 3309040; fax: +7 383 3356684.
E-mail address: dmark@itp.nsc.ru (D.M. Markovich).

0142-727X/$ - see front matter © 2008 Elsevier Inc. All rights reserved.
doi:10.1016/j.ijheatfluidflow.2008.07.005

Nomenclature

Re	Reynolds number
St	Strouhal number
TKE	turbulent kinetic energy
G_θ	axial flux of angular momentum (kg m^2/s^2)
G_z	axial flux of axial momentum (kg m/s^2)
S	swirl rate based on geometry of swirler
Sw	swirl rate based on inflow velocity
U_0	mean flow rate velocity (m/s)
V, W, U	radial, azimuthal, and axial components of mean velocity (m/s)
a	amplitude of forcing (%)
d	nozzle exit diameter (m)
d_0	diameter of nozzle plenum chamber (m)
d_1	centerbody diameter (m)
d_2	external diameter of swirler (m)
r, θ, z	radial, azimuthal, and axial directions in a cylindrical coordinate system
φ	blade angle (rad)
ϕ	phase shift between signals of forcing and data acquisition (rad)
u'_0	average intensity of axial velocity fluctuations at nozzle exit (m/s)
v, w, u	radial, azimuthal, and axial components of fluctuating velocity (m/s)
v', w', u'	intensities of radial, azimuthal, and axial velocity fluctuations (m/s)
ω_θ	azimuthal component of vorticity fluctuations (1/s)
$\langle\rangle$	ensemble averaging operator
$\langle\rangle_\phi$	phase-averaging operator
$*$	indicates instantaneous quantity

For a non-swirling round jet, as for a plane shear layer, it is well known that the formation and downstream evolution of vortices can be controlled by the flow excitation (Crow and Champagne, 1971; Zaman and Hussain, 1981; Broze and Hussain, 1996). It was found that forcing at the prevailing ("natural") frequency gives the strongest increase of the ring-like formation, and thus the greatest turbulent mixing rate in the initial region of the jet. Generally, for the jet "column" the prevailing frequency ranges from $St = 0.3$ to 0.6 (Crow and Champagne, 1971; Hussain and Zaman, 1981; Alekseenko et al., 1997; Drobniak et al., 1998; Vejrazka et al., 2005). The influence of the excitation frequency and amplitude on the behavior of vortex structures was well documented in Broze and Hussain (1996). This excitation promotes the growth of various instability modes (not only fundamental) and provides flow regimes, which are not observed in an unexcited jet. The variety of flow regimes appearing for an excited jet can be explained by the pressured feedback mechanism from the downstream flow events (see Broze and Hussain, 1996). The effect of forcing the free swirling jets at various azimuthal modes was investigated in works by Panda and McLaughlin (1994) and Gallaire et al. (2004). For flow conditions preceding VB, these studies showed that axisymmetric or azimuthal forcing intensifies the development of corresponding instabilities and leads to domination of axisymmetric or helical vortices in the outer mixing layer. For swirling jets with high swirl rates, Gallaire et al. (2004) have shown that VB appears to be insensitive to forcing attempts, at least for the studied parameters. In the work of Khalil et al. (2006), describing the study of the swirling jet at $Re = 600$ with conical VB, the application of high-level forcing at the natural frequency was found to intensify ring-like vortices in the outer mixing layer that resulted in a downstream shift of the VB position. However, the structure of VB almost was not affected. Generally, on the basis of previous works, it can be concluded that combined application of swirl and external forcing can be used as an efficient tool for mixing enhancement in a number of devices utilizing confined jet configurations (chemical reactors, burners, mixing chambers, etc.).

Particle Image Velocimetry (PIV) provides the spatial distributions of instantaneous flow velocity and, consequently, a direct measurement of the spatial velocity derivatives, including vorticity. Besides, PIV can support the storage and processing of extremely large amounts of data that are necessary for reliable calculation of statistical characteristics. This provides a convenient tool for measurement in a turbulent swirling jet with a complex structure. At the same time, for accurate estimation of the above-mentioned quantities, it is necessary to carry out a number of complex pre- and post-processing PIV algorithms. Presently, an iterative cross-correlation approach with image deformation is acknowledged as the most suitable in terms of accuracy and processing time. In Stereo PIV measurements the calibration-based methods with an angular stereoscopic experiment configuration are the most frequently used. Also, an iterative correction procedure can be applied to minimize the error from inaccurate alignment of the laser sheet and calibration target planes. Additional attention should be paid to the PIV data post-processing algorithms before calculation of flow characteristics. As an example, Heinz et al. (2004) have demonstrated that the presence of false vectors in raw data significantly affects the accuracy of calculations of high-order statistical moments. Thus, the stages of raw velocity field validation, false vectors removal (e.g., Westerweel, 1994) and "empty holes" interpolation are needed before stereo reconstruction or further steps of post-processing. As was shown by several authors (Raffel et al., 2007; Foucaut and Stanislas, 2002), the correct calculation of instantaneous velocity gradients requires application of a proper derivative filter in order to minimize both the truncation error linked with the finite form of the filter and the noise error.

The objective of the present work is an experimental study of swirling free turbulent jet flow under the imposition of external axisymmetric velocity fluctuations. The measurements focus on the spatial distributions of the mean flow velocity and turbulent kinetic energy components in the central cross-section of the jet. The Reynolds number of the flow was equal to 8900. Three typical jet configurations were considered: non-swirling jet flow and swirling jet flow with and without pronounced VB. The central point of the present paper is to obtain comprehensive experimental data on the forced turbulent swirling jet by applying an advanced non-intrusive whole-field measurement technique (stereo PIV).

2. Experimental setup, apparatus and data processing

The experimental setup represented a hydrodynamic loop equipped with a rectangular working section (Fig. 1a) made of Plexiglas in order to provide PIV measurements, a pump, a flowmeter and a temperature stabilizing device. Water flow was driven by the pump, the rotation speed of which was precisely controlled by an inverter. A thermostat was used to maintain a constant water temperature of 26 °C with an accuracy of ±0.2 °C. The Reynolds number, defined on the basis of the mean flow rate velocity $U_0 = 0.52$ m/s and nozzle diameter $d = 15$ mm, was equal to 8900. For organization of non-swirling jet flow with a top-hat exit velocity profile, a Vitoshinsky contraction nozzle (see equation below), shown in Fig. 1b, was used (Dyban and Mazur, 1982).

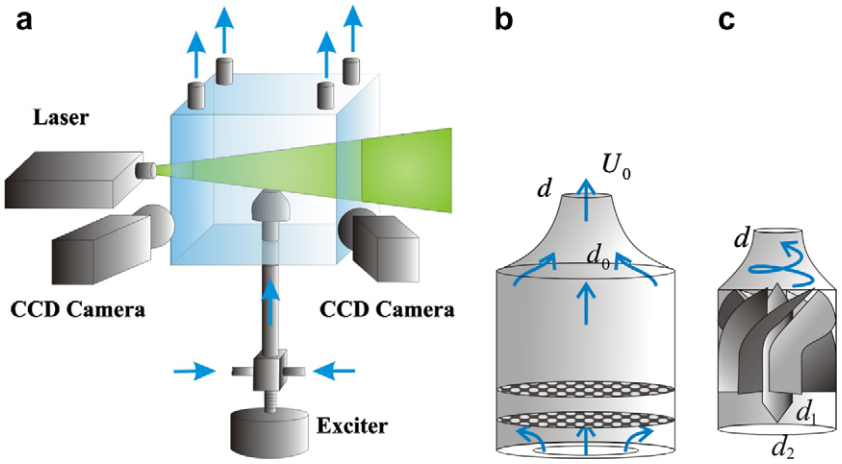

Fig. 1. (a) Working section and stereo PIV system arrangement; (b) sketch of contraction nozzle and (c) scheme of swirler arrangement.

$$r(x) = \frac{1}{2} d_0 \left\{ 1 - \frac{(1-(d_0/d)^2)(1-(x/l)^2)}{(1+(x/l)^2/3)^3} \right\}^{-1/2}. \quad (1)$$

In this equation, l is the length of contraction zone of the nozzle. The diameter of a plenum chamber $d_0 = 65$ mm corresponded to the area contraction rate of 18.8. For swirl organization, smoothing grids in the plenum chamber of the nozzle were replaced by a swirl generator (see Fig. 1c). The definition of the swirl rate is based on the swirler geometry (Gupta et al., 1984):

$$S = \frac{2}{3} \left(\frac{1-(d_1/d_2)^3}{1-(d_1/d_2)^2} \right) \tan(\phi). \quad (2)$$

Here, $d_1 = 7$ mm is the diameter of the centerbody supporting the blades, $d_2 = 27$ mm is the external diameter of the swirler and φ is the blade inclination angle. The following swirl rates were covered $S = 0$, 0.41 and 1.0 by using swirlers with various blade angles. The present swirl rate S is used as the reference for the experimental setup case only. In Section 3.1, some additional attention is drawn to the definition of the swirl rate based on the inflow velocity distributions. The flow conditions and the nozzle setup were similar to the previous study of the impinging swirling jet flow described in Alekseenko et al. (2007b), where more detailed information about the experimental setup can be found.

Jet forcing was applied by perturbing the bulk velocity of the flow by means of an exciter connected to a diaphragm (see Fig. 1a). The diaphragm was mounted to the bottom of a mixing chamber connected to the nozzle plenum chamber by a pipe one meter in length and 20 mm in inner diameter. Due to the symmetrical arrangement of the forcing device, the external flow perturbations were assumed to be axisymmetrical. The amplitude of the sine voltage supplying the exciter was controlled by a power amplifier. Two values of forcing frequency, viz. 18 and 42 Hz, were used, corresponding to the Strouhal numbers $St = 0.52$ and 1.2, respectively. The justification for choosing these forcing frequencies is given in Section 3.1. The measurements were performed in a meridional (central) plane (r, z) passing through the jet axis and covering the initial region of the jet (see Fig. 2).

A "PIV-IT" Stereo PIV system produced at the Institute of Thermophysics was used for the measurements. The system consisted of a double cavity Nd:YAG pulsed laser, two CCD cameras and a synchronizing processor. A laser sheet formed by a system of lenses had a minimal thickness of 0.5 mm in the measurement section. Polyamide particles with mean diameter of 20 μm were used for flow seeding. During the experiments, the system was operated by a computer with "ActualFlow" software, developed in the Institute of Thermophysics and tested during two most recent PIV Challenges (referenced as IOT) in 2003 and 2005 (Stanislas et al., 2005, 2008). For each experimental case, the same parameters were used for image processing, stereo calibration and stereo reconstruction procedures (i.e., interrogation area size, validation parameters, etc.). More detailed information about the PIV system used and some considerations about measurement accuracy are given in Alekseenko et al. (2007a).

For instantaneous two-component (2C) velocity calculation, an iterative cross-correlation algorithm with image deformation was used. The size of the final interrogation area was 32×32 pixels in order to have a low level of noise, and 50% overlap of areas was used. Calculated instantaneous velocity fields were validated, and "outliers" were removed using signal-to-noise criteria for cross-correlation maxima and an adaptive median filter proposed in Westerweel and Scarano (2005). Before stereo reconstruction, the "holes" were interpolated by using a third-order 3×3 linear interpolation filter. Velocity derivatives were calculated from 3C velocity fields by using a second-order centered difference scheme, which is considered to be optimal for 50% of overlap (Raffel et al., 2007; Foucaut and Stanislas, 2002). The final interrogation area size was 1.3 mm, which corresponded to a spatial resolution of 0.65 mm per vector.

In the present stereo configuration the angle between the optical axis of each camera (see Fig. 1a) and the normal of the measurement plane was 30°. The number of image pairs captured by each camera was 1000. A plane calibration target with a size of $50 \times 50\ \text{mm}^2$ was employed for the stereo calibration. Three images of the target located in different normal-to-plane positions were captured: $\{-1.4,\ 0,\ 1.4\ \text{mm}\}$. During the calibration, a third-order polynomial transform was used to minimize non-linear optical distortions. Additionally, to minimize stereo calibration error

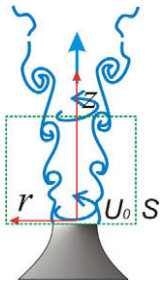

Fig. 2. Sketch of jet flow and measurement area location.

connected with possible misalignment of the laser sheet and target plane, an iterative correction procedure (Coudert and Schon, 2001) was applied. The average value of a disparity map (for definition, see Scarano et al., 2005) was found to be around −12.5 and −0.5 pixels before and after correction, respectively. Parameters of the correction corresponded to the normal-to-plane shift of 0.5 mm of the calibration target and 0.4° rotation around the vertical axis aligned with the center of the target. The maximum difference between distributions of the second-order moments before and after was found to be about 2% in magnitude (see Alekseenko et al., 2007b for details).

Generally, the measurements were performed under the condition of "ensemble" averaging, i.e., during forcing, the frequency of image acquisition (namely, $4\sqrt{2}/3$ Hz) was selected to give an irrational ratio if related to the forcing frequency. This was done to avoid errors connected with sampling effects in measurement of a process with periodical events. Also, phase-averaging (conditional sampling) measurements were made when the forcing frequency was divisible by the acquisition frequency (2.0 Hz). In this case, a phase shift (ϕ) of the sampling event relative to the sine voltage signal was set by the synchronizing processor. Ten phases with a uniform time step were covered. For all measurement cases, 1000 instant velocity fields were measured.

3. Results and discussion

This section presents spatial distributions of the measured instantaneous velocity fields and spatial distributions of the mean velocity and components of turbulent kinetic energy (TKE) for the free swirling jets under unforced and forced conditions. Also, the results of the phase-averaged measurements of the forced swirling jet at $S = 0.41$ are reported. The spatial distributions were calculated on the basis of 1000 measured 3C instantaneous velocity fields. No data smoothing or approximation was performed.

The jets have a general axial symmetry and thus are described using a cylindrical coordinate system. Coordinates (r, θ, z) denote the radial, azimuthal and axial directions, respectively, and (V, W, U) and (υ, w, u) are the radial, azimuthal and axial components of the mean and fluctuating velocity, respectively. In some cases, spatial distributions for the central measurement plane contain negative values of r. This is not typical for the cylindrical coordinates used; thus the following conditions were used for $r < 0$: $u(r) = u(-r)$, $\upsilon(r) = -\upsilon(-r)$, $w(r) = -w(-r)$.

3.1. Flows without forcing

Fig. 3 shows initial distributions of the mean velocity at the nozzle exit. For the non-swirling jet flow the distribution of U is uniform in the jet core. When the swirler for $S = 0.41$ was installed into the nozzle, a peak of the axial velocity appeared at the jet centerline, as in Billant et al. (1998). Liang and Maxworthy (2005) showed that the central over-shoot of the axial velocity appears for a swirling flow passing through a contraction nozzle. For the case $S = 1.0$, the axial velocity profile reaches negative values at the nozzle exit. This corresponds to the recirculation zone caused by the VB with the stagnation point located within the nozzle. Liang and Maxworthy (2005) used a non-contracting nozzle to produce nearly uniform distributions of axial velocity from a rotating honeycomb. This was done to achieve similarity in inflow profiles of the axial velocity for the different swirl rates to allow accurate study of the swirl rate for which the VB appears. In the present study, attention is focused on analysis of flow forcing applied to two different, but frequently encountered configurations of turbulent swirling jet – with and without clearly definable VB. Thus, the realized velocity profiles are typical for a number of practical cases.

When the distributions of the initial velocity are measured, the swirl rate Sw (e.g. Van Slooten and Pope, 1999) can be defined as the ratio of the axial flux of angular momentum (G_θ) to the axial flux of axial momentum (G_z):

$$Sw = \frac{2G_\theta}{dG_z}, \tag{3}$$

$$G_\theta = \int_0^{d/2} \rho U W r^2 \, dr, \quad \text{and} \quad G_z = \int_0^{d/2} \rho U^2 r \, dr, \tag{4}$$

For the cases studied (geometrically defined swirl rates are $S = 0.41$ and 1.0), the values of Sw were found to be 0.44 and 0.79, respectively. This difference can be explained by noting that S in Eq. (2) was obtained based on the assumption of uniform velocity distributions in the radial direction inside of a swirler. Also, the shape of swirler's blades and possible flow separation after the swirler's centerbody were not taken into account in (2). It is important to notice that another definition of the swirl rate is often used (for example, in Billant et al., 1998, and Khalil et al., 2006), one based on values of $U(r = 0)$ and $W(r = d/4)$ (or a maximum value of W). We do not use this definition in the present study, because additional experiments showed that the distributions of initial velocity profiles for the cases with and without VB were essentially different, in contrast to the data of Billant et al. (1998). Also, in the previous work by Alekseenko et al. (2007a), it was shown that initial velocity profile is affected by not only the nozzle characteristics but also the peculiarities of the surrounding space. Thus, significantly different distributions of U were observed for the free swirling jet and impinging swirling jet with a plate located three nozzle diameters downstream, while the jets were organized by the same nozzle with $S = 0.41$ geometry. For this reason, the definition of the swirl rate based on integral characteristics of inflow velocity was used in the present study.

Fig. 4 shows spatial distributions of the axial mean velocity and the axial component of turbulent kinetic energy (TKE) measured

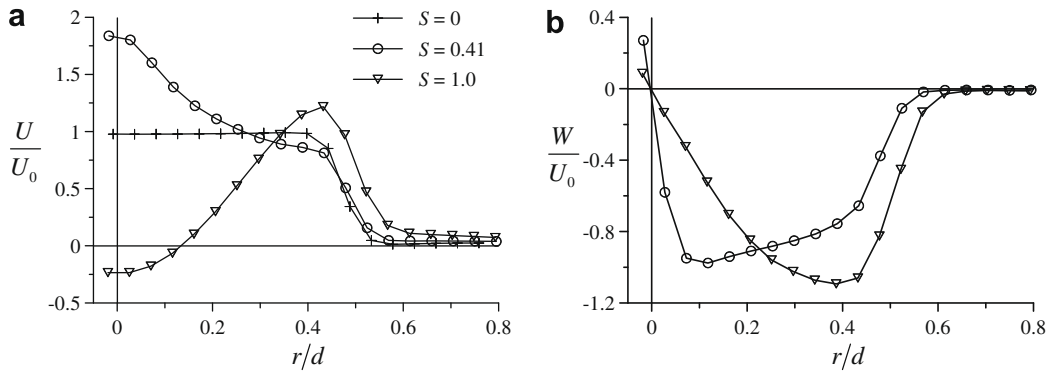

Fig. 3. Distributions of the (a) axial and (b) azimuthal mean velocity near the nozzle exit ($z/d \approx 0.04$) for unforced free jets ($St = 0$).

for the non-swirling jet. The colorscale for $\langle u^2 \rangle$ is selected to fit maximum values for the swirling jet cases (see Figs. 5 and 6). Examples of instantaneous velocity and vorticity fields are also shown in Fig. 4c to demonstrate the structure of vortices emerging in the non-swirling jet flow.

The scenario of vortex formation in the initial region of axisymmetric non-swirling jets is well acknowledged. According to linear stability models, for the *th*-like velocity profile, the axisymmetric mode has the greatest increment only in the vicinity of the nozzle exit. Growth of Kelvin–Helmholtz instabilities leads to the vortices' formation, resulting in an increase of the TKE in the mixing layer. Downstream, at a distance of one to two nozzle diameters, the different spiral modes start to dominate. The structure of vortices and instabilities in swirling jets is known to be significantly more complex: starting from the nozzle exit, helical waves of different modes are dominant with an increase of swirl intensity.

Flow characteristics for the case $S = 0.41$ are presented in Fig. 5. The local minimum of $U = 0.07U_0$ is observed for the axial mean velocity within the jet core at $z/d = 1.1$. The positive value of the mean axial velocity indicates the absence of a stable recirculation zone, and no clear VB could be determined from the average velocity field. At the same time, as is seen from instantaneous velocity fields (the example is shown in Fig. 5c), the local weak reserve flows exist near the jet axis. Strong shear of the axial velocity near the jet axis produced intense vortices, which were observed to have a helical structure. The vortices resulted in the local

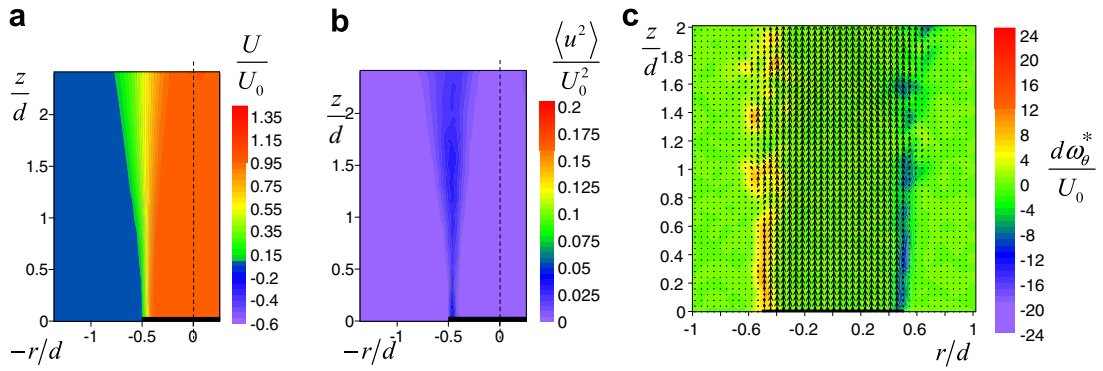

Fig. 4. Spatial distributions of the (a) axial mean velocity, (b) axial component for TKE and (c) instantaneous velocity and vorticity fields for an unforced jet at $S = 0$.

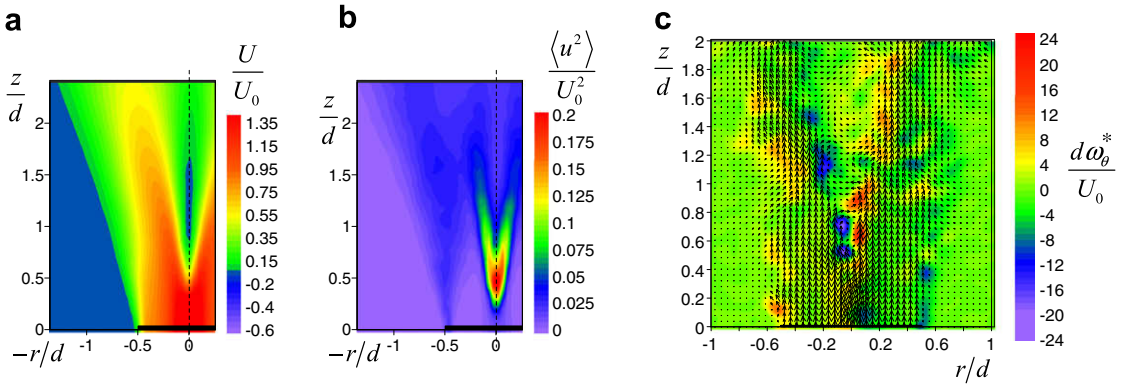

Fig. 5. Spatial distributions of the (a) axial mean velocity, (b) axial component for TKE and (c) instantaneous velocity and vorticity fields for an unforced jet at $S = 0.41$.

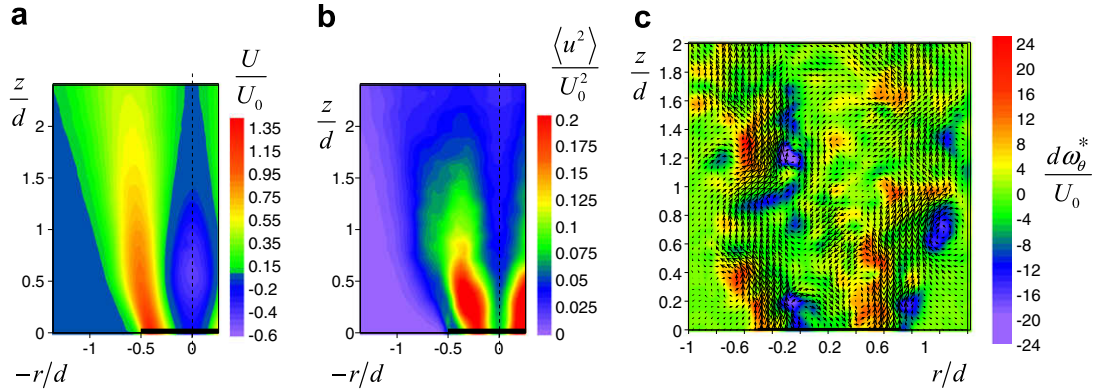

Fig. 6. Spatial distributions of the (a) axial mean velocity, (b) axial component for TKE and (c) instantaneous velocity and vorticity fields for an unforced jet at $S = 1.0$.

maximum of the axial component of TKE $\langle u^2 \rangle = 0.22U_0^2$ at $z/d = 0.5$ just past the position of maximal decay rate of the axial velocity ($z/d = 0.44$). Less pronounced helical vortices were also observed in the jet outer mixing layer, where the greatest value of $\langle u^2 \rangle$ was 0.04 $\langle U_0^2 \rangle$.

For the swirling jet at $S = 1.0$ (Fig. 6), the VB has a much more pronounced character, and a recirculation zone was found to extend in the whole initial region of the jet, up to $z/d = 1.8$. The mean axial velocity had the negative minimum value of $U = -0.48U_0$ at $z/d = 0.6$. Analyzing the structure of large-scale vortices in the measurement plane, one can conclude that the vortices emerging inside the recirculation zone and in the outer mixing layer are significantly more powerful than in the two previous cases. That observation is reflected in the distributions of the axial component of TKE plotted in Fig. 6b. The helical structure of the vortices was found to be quite similar to the observations by Liang and Maxworthy (2005) for the jet at $S = 0.9$ and $Re = 1000$. Obviously, in the present work, the flow is turbulent; thus, a band of azimuthal modes with different magnitudes exists in the flow. However, at each instant of time (see the snapshot in Fig. 6c), one can clearly identify two vortices of opposite sign linked together. One vortex is located inside the recirculation zone, while the other vortex is outside. Considering left and right sides of the jet, the vortex pairs propagate asymmetrically, indicating an odd mode for the inner and outer helix.

According to the time-resolved measurement made by Liang and Maxworthy (2005), the mode of the helices is expected to be $m = 1$. Similar structure was found in Cala et al. (2005) for the conditional sampled measurements in the swirling jet at $Re = 15{,}000$ and $S = 1.01$. The authors found two inner and outer spiral secondary vortices induced by precession of the jet swirling core. In the present paper, the helical vortex inside the recirculation zone was found to give a major contribution to the axial component of TKE. As can be seen from Fig. 6c, $\langle u^2 \rangle$ reaches a value of $0.25U_0^2$ at the edge of the recirculation zone. A detailed study of the vortices' structure and development of instabilities would require analysis of the time-resolved ensemble of instantaneous 3C velocity distributions, but that is not the aim of the present study.

In the following sections, the response of the swirling jets to the application of the external forcing is considered. The "axisymmetric" (i.e., with azimuthal mode 0) forcing was applied at $St = 0.52$ and 1.2 with various amplitudes. In our previous studies, where a similar nozzle setup was used, the range of frequencies corresponding to $St = 0.4–0.7$ was found to be preferable for the forcing (Alekseenko et al., 1997) of the non-swirling jet flow. Thus, the forcing at $St = 0.52$ was selected for strengthening the ring-like vortices generation in the jets with $S = 0$ and 0.41. The other value of the Strouhal number, $St = 1.2$, was chosen on the basis of preliminary calculated one-dimensional spatial spectra, obtained from PIV velocity fields measurements. For the spectra estimation, additional experiments were performed with twice the spatial resolution, viz. 0.34 mm per vector. The most representative spectra are shown in Fig. 7. For the case $S = 0.41$, a slightly visible peak is observed for F_{rr}. The peak position is $k_z d \approx 11$, corresponding to $St \approx 1.8$, calculated on the basis of mean flow rate velocity U_0, and to $St \approx 3.1$, where the mean centerline velocity U at the nozzle exit ($r = 0$, $z = 0$) was taken as the velocity scale. This frequency is considered to correspond to the strong helical vortex structures developing near the jet axis (see Fig. 5c). However, forcing of helical instabilities was not the aim of the present study; thus, this frequency was not considered. For the case $S = 1.0$, a more pronounced peak at $St \approx 1.2$ (the mean flow rate velocity U_0 was used for the scaling) was found in the spectra calculated across the jet in the area of the recirculation zone ($z/d \approx 0.5$). This peak was interpreted as corresponding to the precession of the recirculation zone which dominates the whole flow. Thus, the forcing at $St = 1.2$ was also applied to investigate the ability of turbulent mixing control in the swirling flow with pronounced VB; this state was found to have the highest mixing rate among the studied jet flows.

3.2. Forcing effect on jet without swirl

Measured spatial distributions of the mean velocity and TKE components for the forced non-swirling jet are reported in the present section. The effect of the two forcing frequencies, corresponding to $St = 0.52$ and 1.2, on the instantaneous velocity fields and TKE distributions is analyzed for the various amplitudes of forcing.

3.2.1. Inflow distributions

It was found that the forcing has almost no effect on the mean velocity profiles at the nozzle exit and only weakly affects spatial distributions of the mean velocity downstream. Thus, the data on the initial mean velocity in the present paper are limited to Figs. 3, 4a and 11. Intensities of velocity fluctuations near the nozzle exit are shown in Fig. 8. For the unforced flow, u', v' and w' were found to be around 3.5%, 5.5% and 6% of U_0 in the jet core, respectively. The maximum value of $u' = 0.21U_0$ was observed at $r/d \approx 0.5$, which was almost unaffected by forcing at a low amplitude. It was observed that forcing has either great or weak effect on the jet structure, depending on the amplitude. As the reference for the forcing amplitude at the frequency used, the normalized intensity $a = (u'_0/U_0) \times 100\%$ of the axial velocity fluctuations at the nozzle exit in the case of the non-swirling jet was used for the all studied jet flow configurations. The non-swirling jet was selected because, for this case, the low-amplitude forcing increases

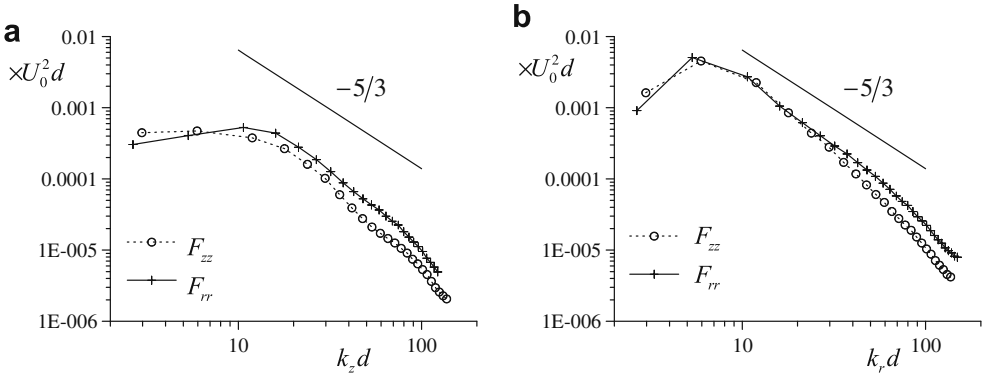

Fig. 7. One-dimensional spatial spectra calculated for swirling jets without forcing ($St = 0$). (a) $S = 0.41$, calculated along the jet axis; (b) $S = 1.0$, calculated in the radial direction ($z/d = 0.5$ cross-section).

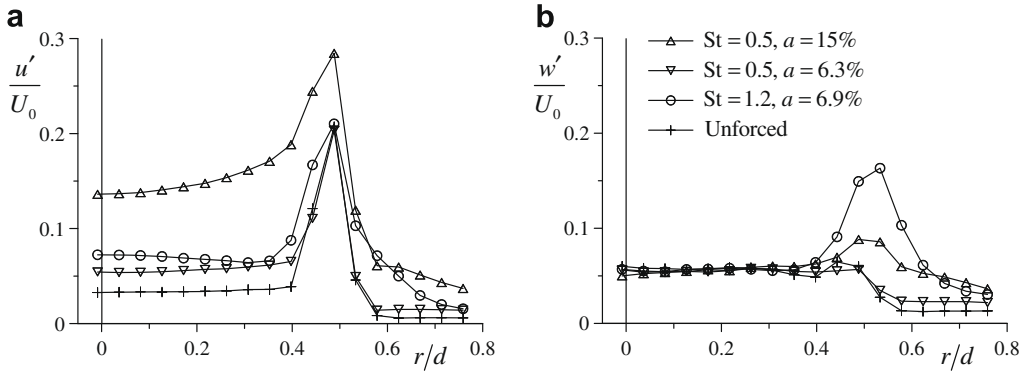

Fig. 8. Intensities of the (a) axial and (b) azimuthal velocity fluctuations near the nozzle exit ($z/d \approx 0.04$) for a non-swirling jet.

intensity of axial velocity fluctuations almost uniformly for $r/d < 0.4$ (see Fig. 8a) and has rather weak influence on intensity of the radial and azimuthal fluctuations in the jet core. For all cases, distributions of intensity of the radial velocity fluctuations υ' were found to be quite similar to those for the azimuthal fluctuations w'; thus, υ' distributions are not presented in the paper. Values of u'_0 were obtained by averaging intensities u' over $r/d < 0.4$. For the jet without forcing, u'_0/U_0 was found to be 0.033 (i.e., $a = 3.3\%$).

In the experiments, the highest values of forcing amplitude a were 27% and 10% for frequencies $St = 0.52$ and 1.2, respectively. By analyzing initial distributions for the non-swirling case, it was found that, for forcing amplitudes greater than 9% for $St = 0.52$ and 5% for $St = 1.2$, respectively, the shape of the distributions of the radial and azimuthal intensities significantly differs from those for unforced case (see Fig. 8b), in spite of the fact that excitation had only an axial mode. Also, for these amplitudes, the forcing increases the value of u' not only in the jet core; rather, the whole shape of the distributions is changed. These facts manifest the nonlinear mechanisms of instabilities growth; thus, the imposed perturbations at these amplitudes were considered to be high.

3.2.2. Spatial distributions

The examples of instantaneous velocity and vorticity fields are presented in Fig. 9 for the forced jet at relatively high amplitudes. The distributions are normalized by the nozzle diameter d and by the mean flow rate velocity U_0. In general, forcing at both frequencies led to a quasi-periodical formation of the large-scale ring-like vortices appearing in the vicinity of the nozzle exit, while for the unforced jet clearly identifiable vortices were observed far downstream, at $z/d > 0.8$ (see Fig. 4c). The distance between the propagated vortices was near equivalent and inversely proportional to the forcing frequency. Fig. 10 shows examples of spatial distributions of the radial, axial and azimuthal components of TKE for the non-swirling jet with and without forcing. The forcing at $St = 0.52$ caused a significant increase of in-plane TKE components in the mixing layer (namely of $\langle u^2 \rangle$ and $\langle \upsilon^2 \rangle$) due to the enhanced generation of ring-like vortices, while $\langle w^2 \rangle$ increased slightly. As expected, the flow response to $St = 1.2$ forcing was found to be less pronounced, in agreement with a number of previous investigations. The highest value of TKE component obtained was found for the radial TKE in the case of forcing at $St = 0.52$, $a = 15\%$: $\langle \upsilon^2 \rangle = 0.13 U_0^2$ reached in the mixing layer at $z/d = 0.6$.

The downstream evolution of the axial mean velocity for the unforced jet is shown in Fig. 11. Application of forcing changed the mean velocity distribution insignificantly: a slightly greater spreading rate was observed (not shown in the figure).

Further, only the distributions of the radial component of TKE are considered in more details. The radial component was selected because it is the most representative of the increase of the in-plane TKE components caused by forcing. Radial distributions of $\langle \upsilon^2 \rangle$ for the various cross-sections of the unforced and forced jets at $St = 0.52$ are shown in Fig. 12. With an increase in z/d, values of $\langle \upsilon^2 \rangle$ were almost entirely unchanged in the jet core and rapidly increased in the mixing layer. In case of the unforced flow, a peak of $\langle \upsilon^2 \rangle$ was observed at the distance of $z/d \approx 1.6$ (see spatial distributions in Fig. 10), after which $\langle \upsilon^2 \rangle$ decreased in magnitude downstream and became smoother due to the diffusion effects. For the forced flow case at $a = 6.3\%$, the maximum value of $\langle \upsilon^2 \rangle$ increased from $0.017 U_0^2$ to $0.073 U_0^2$ (see Fig. 10b), while the initial distribution of $\langle \upsilon^2 \rangle$ remained almost unchanged. A significant increase of TKE indicates a higher turbulent mixing rate for the jet under the forced conditions. Fig. 13a shows radial distributions of $\langle \upsilon^2 \rangle$ for the various forcing amplitudes. The cross-section $z/d = 1.0$ was selected as the most representative. A maximum value of $\langle \upsilon^2 \rangle$ in-

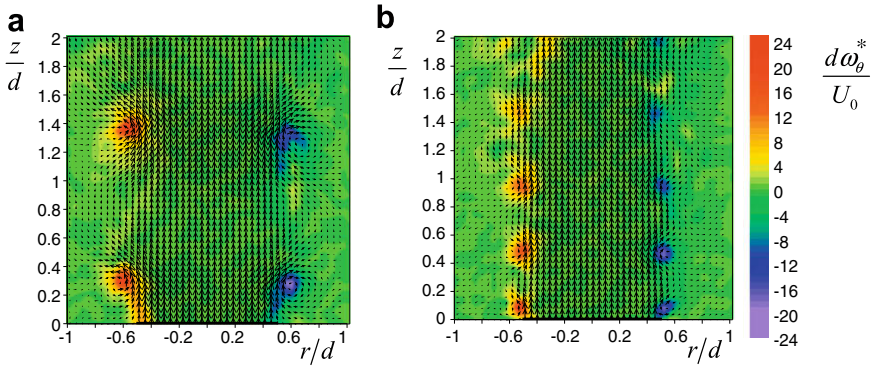

Fig. 9. Examples of instantaneous velocity and vorticity fields for a free jet at $S = 0$. (a) $St = 0.52$, $a = 15\%$ and (b) $St = 1.2$, $a = 6.9\%$.

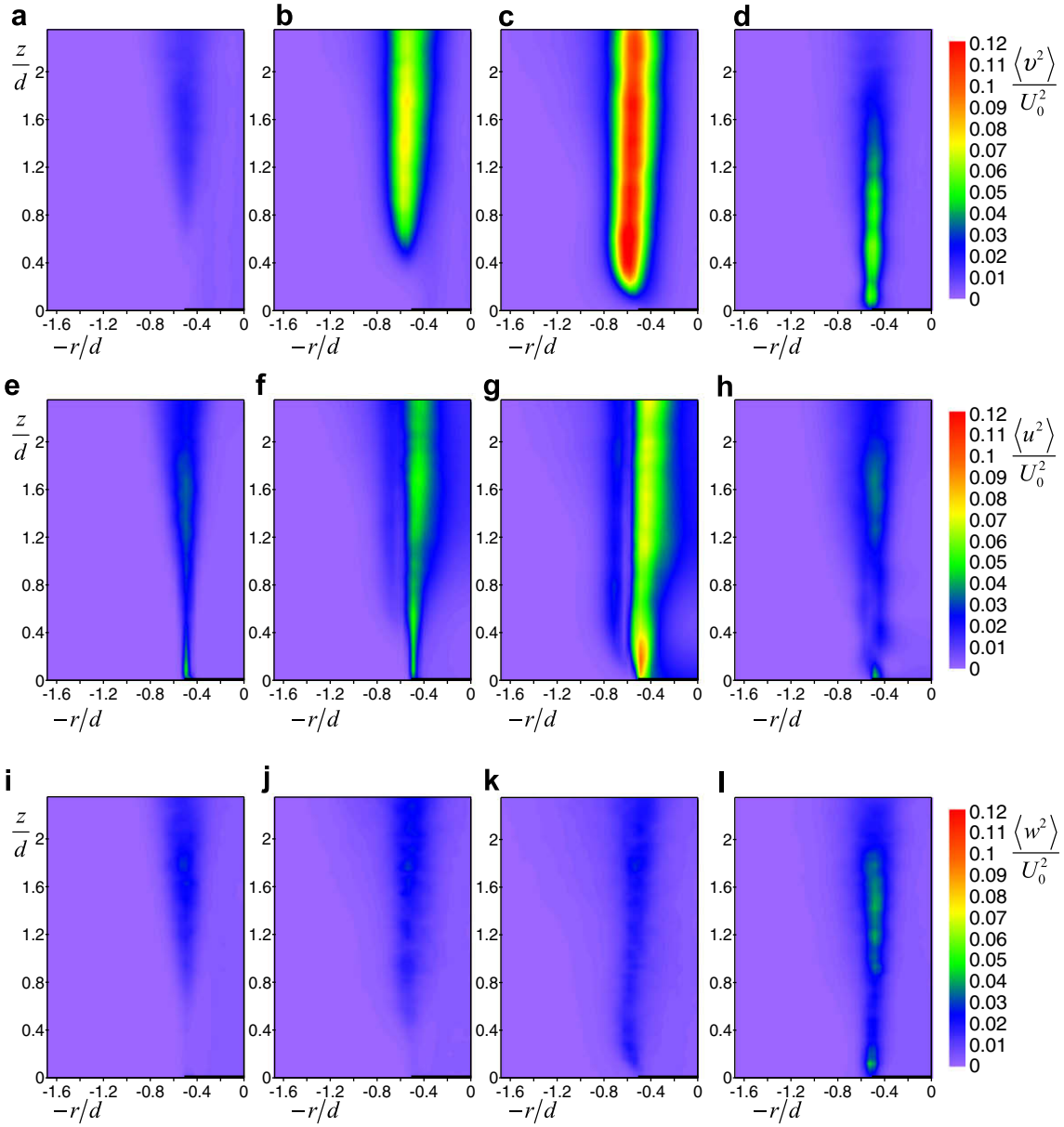

Fig. 10. Components of TKE for the free jet at $S = 0$. (a), (e), (i): $St = 0$; (b), (f), (j): $St = 0.52$, $a = 6.3\%$; (c), (g), (k): $St = 0.52$, $a = 15\%$; (d), (h), (l): $St = 1.2$, $a = 6.9\%$.

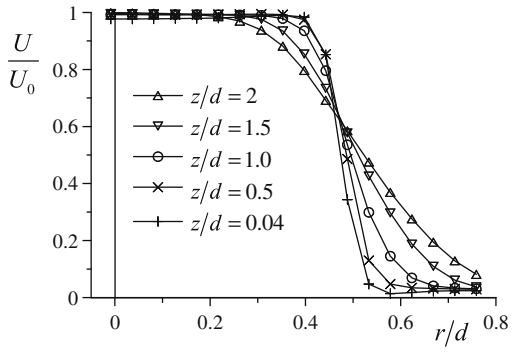

Fig. 11. Radial distributions of the axial mean velocity across an unforced free jet at $S = 0$.

creased with growth in a and reached the value of $0.12U_0^2$ for the case of $a = 15\%$ (not shown in Fig. 13a). The position of the maximum also was found to shift towards a greater value of r/d. Growth of $\langle \upsilon^2 \rangle$ along the mixing layer is shown in Fig. 13b for the various amplitudes of forcing at $St = 0.52$ ($r/d = 0.58$, where the highest growth rate of TKE components was found, was selected). For small values of z, $\langle \upsilon^2 \rangle$ can be approximated by the exponential function $A \times \exp(Bz/d)$, where B is the growth rate. One can observe that the growth rate B increased by almost two times: from 7.6 for the unforced and 15.7 for the forced jet (see Fig. 14).

3.3. Forcing effect on jet with low swirl rate

This section reports the results of the forcing effect on the swirling jet flow at the low swirl rate $S = 0.41$. Inlet distributions of velocity fluctuations as well as the spatial distributions of the TKE components and instantaneous velocity fields are presented for the various forcing conditions. More detailed experimental data about the radial component of TKE are given for the case of forcing at $St = 0.52$. Also, the results of the phase-averaged measurements coupled with periodical forcing are presented in Section 3.3.3.

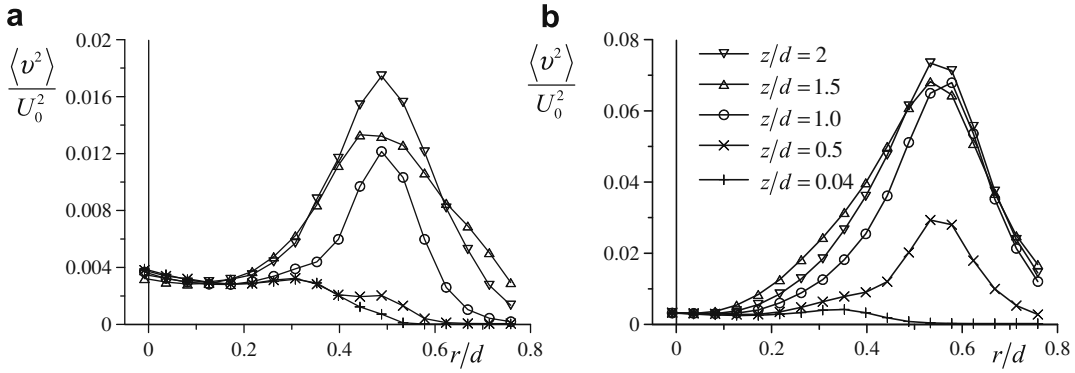

Fig. 12. Radial distributions of the radial component of TKE across a free jet at $S = 0$. (a) Unforced jet and (b) $St = 0.52$, $a = 6.3\%$.

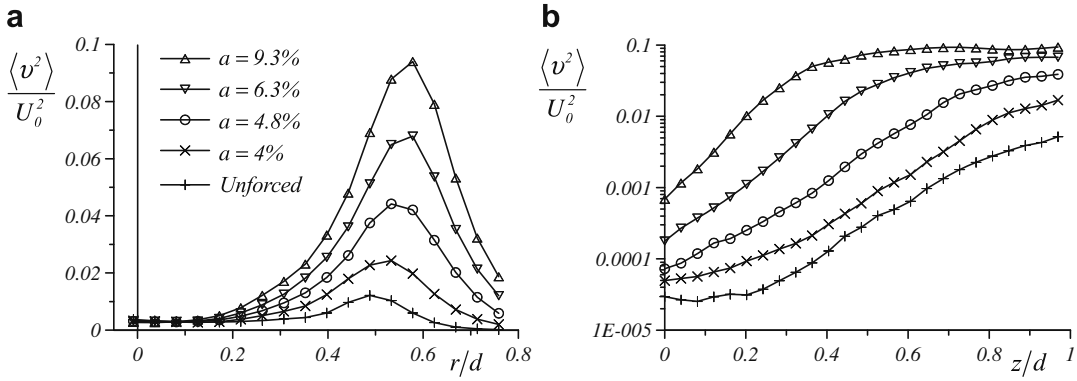

Fig. 13. Effect of forcing amplitude ($St = 0.52$) on the radial component of TKE in a free jet at $S = 0$. Cross-sections: (a) $z/d = 1$ and (b) $r/d = 0.58$.

3.3.1. Inflow distributions

Initial distributions of u' and w' for a swirling jet with $S = 0.41$ are presented in Fig. 15a and b. As for the jet with $S = 0$, the most representative cases of forcing conditions are shown. The distributions of υ' are similar to intensity of the azimuthal fluctuations w' and thus are not presented. The magnitude and shape of distributions of the intensities are significantly different from the case of the non-swirling jet. For the unforced case at $S = 0.41$, u'_0 was found to be approximately two times greater than for the case $S = 0$, i.e., 7.3% of U_0. The effect of forcing on the initial distributions of fluctuation intensities was quite similar to the $S = 0$ case. The influence of forcing on w' was observed near the nozzle edge only at relatively great amplitudes. Forcing at low amplitude caused an increase in the magnitude of u' in the jet core, while the value of a local maximum at $r/d \approx 0.5$ was almost unchanged. Also, the forcing effect was found to be more pronounced near the jet axis; that can be explained by the effect of local separation after the swirler's centerbody.

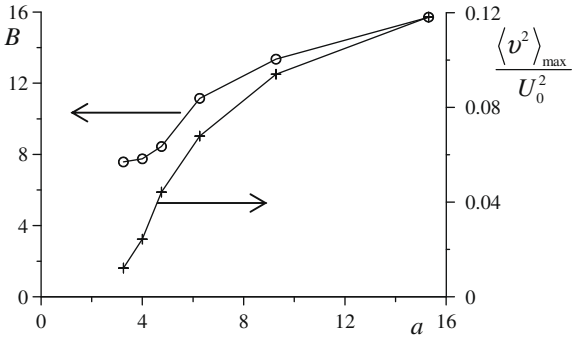

Fig. 14. Effect of forcing amplitude ($St = 0.52$) on the growth rate at $r/d = 0.58$ and maximum value at $z/d = 1$ of the radial component of TKE in a free jet at $S = 0$.

3.3.2. Spatial distributions

As with the non-swirling jet, forcing has a minor effect on the mean velocity, and thus it is not plotted. Spatial distributions of the radial, axial and azimuthal components of TKE for the forced swirling jet at $S = 0.41$ are shown in Fig. 16. It was observed that the forcing caused a significant increase of $\langle u^2 \rangle$ and $\langle \upsilon^2 \rangle$ in the outer mixing layer, while $\langle w^2 \rangle$ did not strongly increase. The flow response to the forcing at $St = 1.2$ was found to be less pronounced for the whole range of amplitudes studied. In addition, if one compares the cases of $S = 0$ and 0.41, the non-swirling jet is more sensitive to the forcing than the jet at $S = 0.41$. In the case of $St = 0.52$ forcing at $a = 15\%$, the maximum value of $\langle \upsilon^2 \rangle$ in the mixing layer was $0.09U_0^2$ at $z/d = 0.32$, about one-and-a-half times lower than the maximum observed for non-swirling flow. Besides, the forcing at $St = 0.52$ led to a clearly visible decrease of radial and azimuthal components of turbulent kinetic energy in the jet centerline, while $\langle u^2 \rangle$ increased slightly.

The forcing effect on the structure of vortices in the flow is demonstrated by the examples of the spatial distributions of normalized instantaneous velocity and vorticity fields plotted in Fig. 17. For both forcing frequencies, nearly axisymmetric (ring-like) large-scale vortices dominate in the outer mixing layer. As with the non-swirling jet case, forcing at $St = 0.52$ leads to more pronounced generation of ring-like vortices (which can be clearly identified up to $z/d = 1.2$) than in case of the forcing at $St = 1.2$. This is reflected in Fig. 16 by the increase of $\langle u^2 \rangle$ and $\langle \upsilon^2 \rangle$ values in the outer mixing layer. Also, it can be seen that for the case of $St = 0.52$,

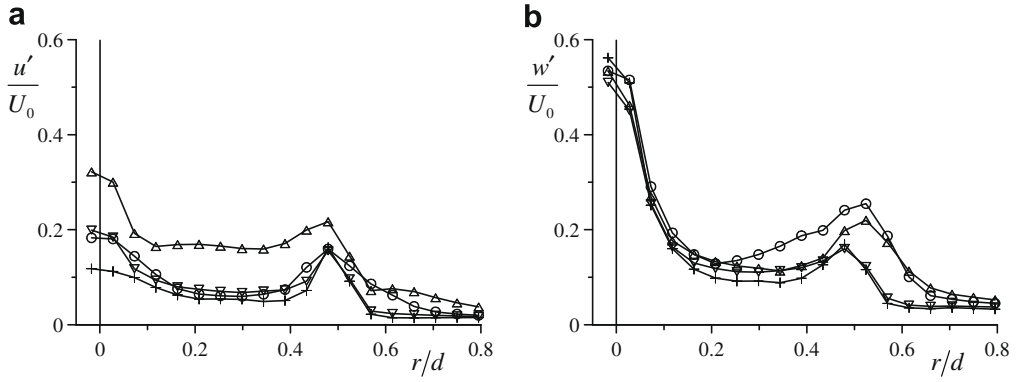

Fig. 15. Intensities of the (a) axial and (b) azimuthal velocity fluctuations near the nozzle exit ($z/d \approx 0.04$) for a swirling jet at $S = 0.41$. See Fig. 8 for the legend.

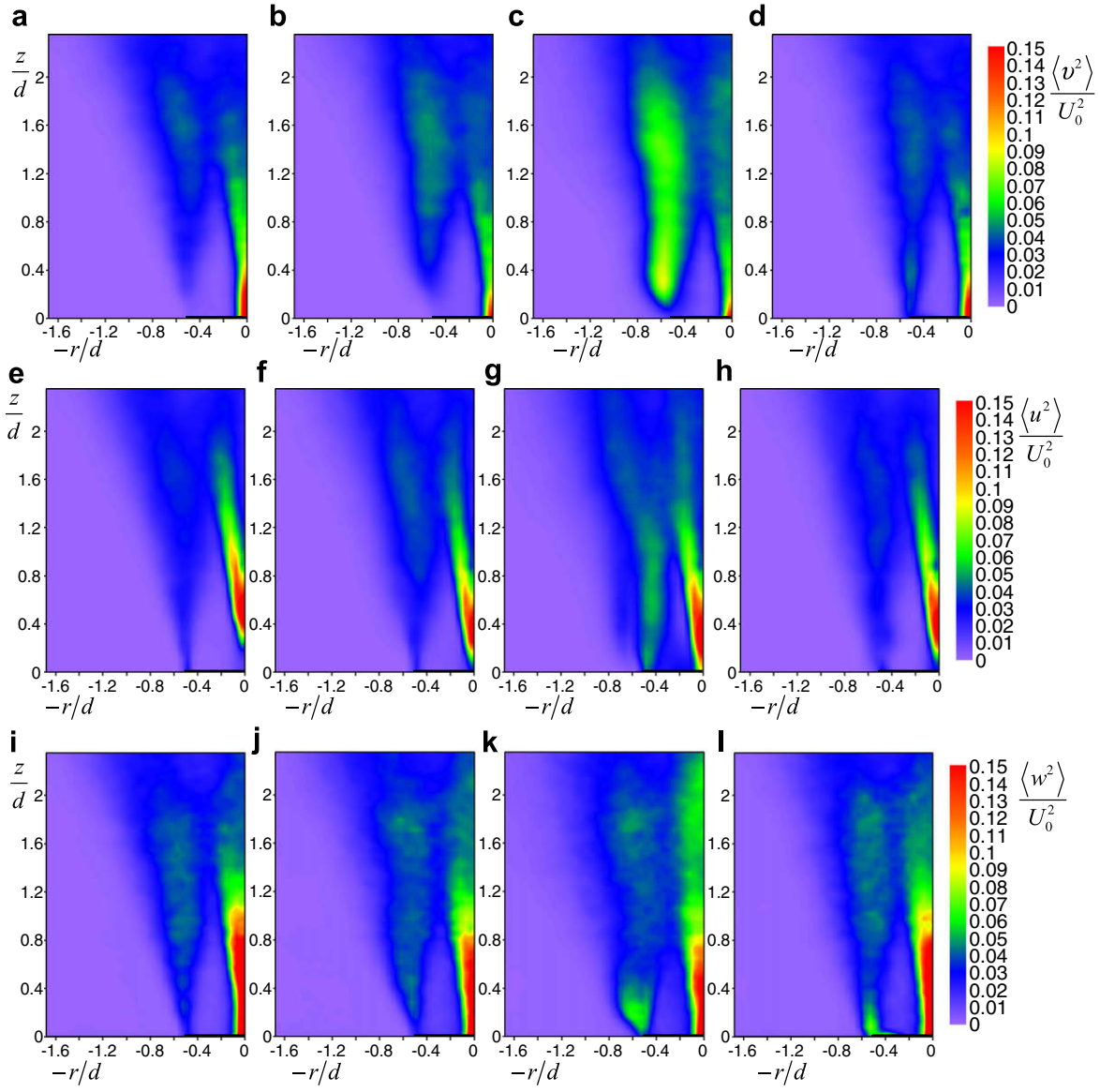

Fig. 16. Components of TKE for a free jet at $S = 0.41$. (a), (e), (i): $St = 0$; (b), (f), (j): $St = 0.52$, $a = 6.3\%$; (c), (g), (k): $St = 0.52$, $a = 15\%$; (d), (h), (l): $St = 1.2$, $a = 6.9\%$.

intensity of the vortices near the jet axis is decreased. This is also manifested on the distributions of TKE components shown in Fig. 16. One can conclude that forcing under the tested conditions significantly affects only the outer mixing layer of the weakly swirling jet, while the effect on the flow structure near the jet centerline is minor.

The evolution of the axial and azimuthal mean velocity distributions with axial direction is shown in Fig. 18 for the unforced flow.

In contrast to the non-swirling jet, a greater spreading rate and fast decay of the longitudinal velocity are observed for the swirling jet at $S = 0.41$. Both azimuthal and axial mean velocity become smoother downstream, and the Sw calculated for the $z/d = 2$ cross-section was found to be 0.5.

Radial distributions of the radial component of TKE for the various cross-sections are shown in Fig. 19. Flow regimes of the forced at $St = 0.52$ and $a = 15\%$ and unforced jet are compared. With z/d increase, rapid decay of the centerline peak of $\langle \upsilon^2 \rangle$ was observed in both cases. The maximum of $\langle \upsilon^2 \rangle$ observed in the mixing layer at $r/d \approx 0.6$ and $z/d \approx 0.5$ is equal to $0.026U_0^2$ and to $0.081U_0^2$ for the unforced and forced cases, respectively. Further downstream, $\langle \upsilon^2 \rangle$ demonstrated quite uniform distributions, which were about one-and-a-half times greater in magnitude for the forced case.

Fig. 20a shows radial distributions of $\langle \upsilon^2 \rangle$ at the $z/d = 0.5$ cross-section for the various forcing amplitudes. In the outer mixing layer, the maximum value $\langle \upsilon^2 \rangle = 0.081U_0^2$ was observed for the case of $a = 15\%$. As with the non-swirling jet, the position of the maximum shifted towards a greater value of r/d with increasing a. Growth of $\langle \upsilon^2 \rangle$ along the center of the mixing layer ($r/d = 0.61$) is shown in Fig. 20b for $St = 0.52$. As with the non-swirling jet, $\langle \upsilon^2 \rangle$ was well fit by an exponential function in the initial region of the jet. Fig. 21 shows the growth rate B and values of $\langle v^2 \rangle$ peak in the outer mixing layer from Fig. 20a. The growth rate was found to be almost constant, i.e., $B \approx 13$, for the all cases. Monotonous growth in the amplitude of the peak value of the $\langle \upsilon^2 \rangle$ was observed; however, the values were found to be less than for the non-swirling jet.

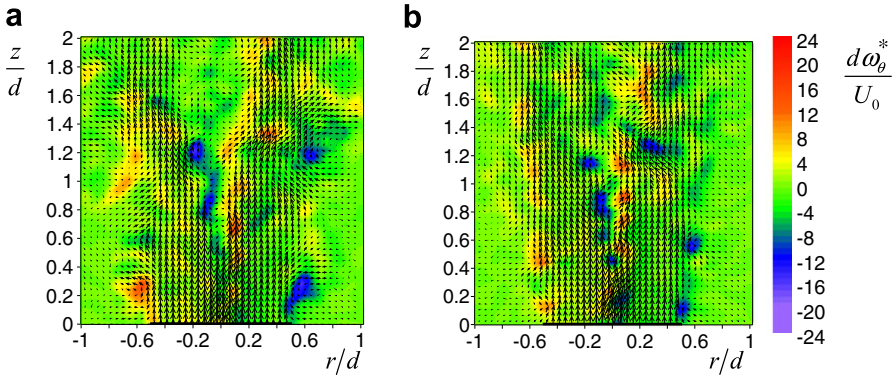

Fig. 17. Examples of instantaneous velocity and vorticity fields for a free jet at $S = 0.41$. (a) $St = 0.52$, $a = 15\%$ and (b) $St = 1.2$, $a = 6.9\%$.

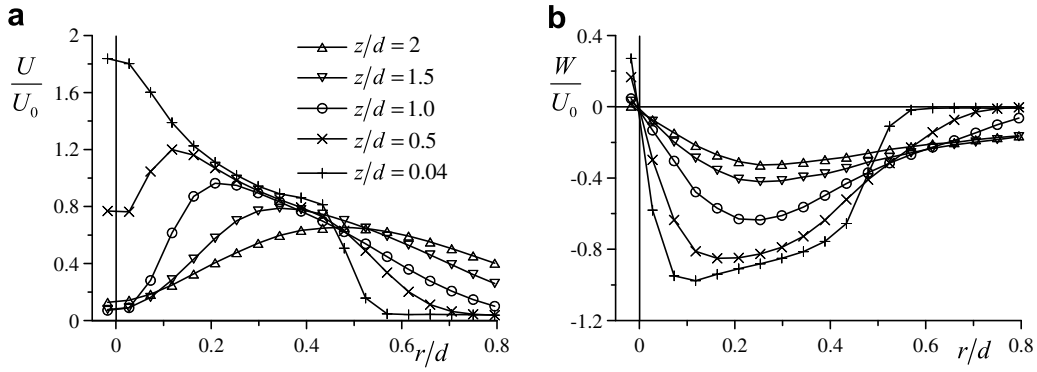

Fig. 18. Radial distributions of the (a) axial and (b) azimuthal mean velocity across an unforced free jet at $S = 0.41$.

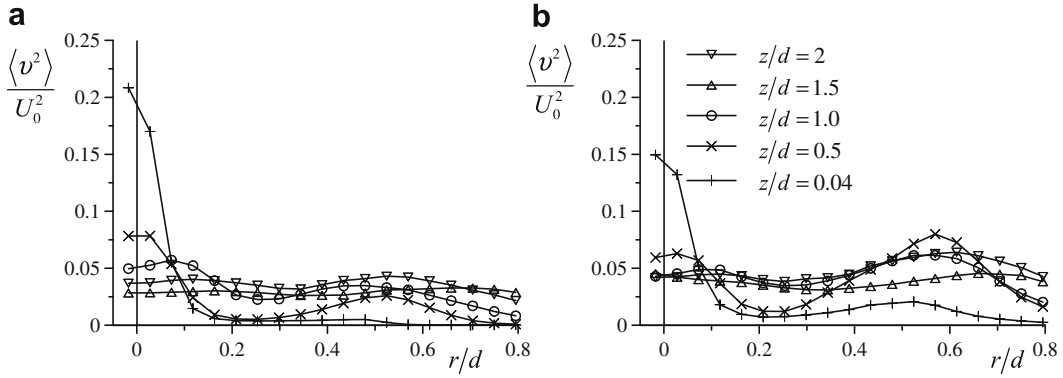

Fig. 19. Radial distributions of the radial component of TKE across a free jet at $S = 0.41$. (a) Unforced jet and (b) $St = 0.52$, $a = 15\%$.

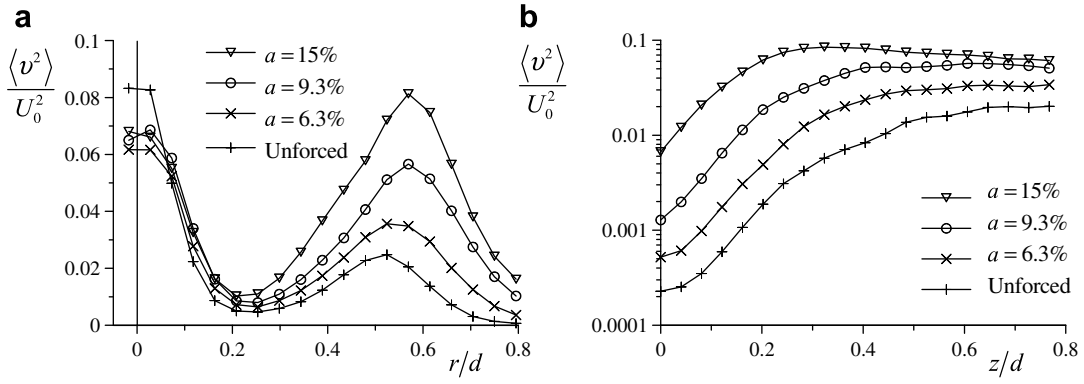

Fig. 20. Effect of forcing amplitude ($St = 0.52$) on the radial component of TKE in a free jet at $S = 0.41$. (a) $z/d = 0.5$ and (b) $r/d = 0.61$ cross-sections.

3.3.3. Conditional sampling results

This section demonstrates the results of the phase-averaged measurements for the swirling jet at $S = 0.41$. As was shown above, the forcing at both frequencies produces quasi-periodical large-scale ring-like vortices in the outer mixing layer. In this context, a conditional sampling technique was applied for the forcing at $St = 0.52$ with $a = 6.3\%$. Fig. 22 presents spatial distributions of the normalized mean velocity, vorticity (in normal-to-measurement plane direction) and TKE components measured with a phase-averaging approach for the forced swirling jet at $S = 0.41$. It should be noticed that large-scale structures of positive values (corresponding to the rotation in counter-clockwise direction) are identifiable on the phase-averaged vorticity fields up to $z/d \approx 2$. Analyzing the lengthy zone of negatively-signed vorticity corresponding to the helical vortices found near the jet axis (see Figs. 5c and 17), it is apparent that the periodical forcing does not produce quasi-periodical structures in the inner mixing layer of the jet. By examining the phase-averaged vorticity and azimuthal velocity fields, one can conclude that fluid inside large scale vortices mainly rotates in the same directions as the mean flow; however, this velocity is slightly lower. The spatial distributions of phase-averaged TKE components show that the greatest values of the velocity fluctuations are observed in the regions with a high gradient of the phase-averaged velocity. All distributions of the phase-averaged TKE components are in correlation with the vorticity plots and show locally large values (up to $0.06U_0^2$ for $\langle \upsilon^2 \rangle_\phi$ and $\langle u^2 \rangle_\phi$) in the vicinity of the "frozen" large-scale vortices.

Figs. 23 and 24 show profiles of the phase-averaged azimuthal vorticity and radial velocity component along the mixing layer at the $r/d = 0.61$ cross-section. Two phases differing by π are shown as the most representative cases. From Fig. 23a one can identify large-scale vortices propagating along the jet mixing layer. The magnitude of the vorticity increased at the initial region (up to $r/d < 0.4$) of the jet and decreased downstream. The maximum value of the normalized phase-averaged vorticity was 10 at $z/d = 0.4$. The ensemble-averaged vorticity had a maximum of 3.1 in the same location.

Profiles of the phase-averaged components of TKE along the mixing layer are presented in Fig. 24 for the same cross-section as in Fig. 23. As with the spatial distributions, local maxima, most pronounced for $\langle u^2 \rangle_\phi$, are observed in the regions of the large-scale vortices. By comparing the two shown phases, one can conclude that the contribution of the regular structures to the TKE components can be up to 2.7 times greater than "background" fluctuations.

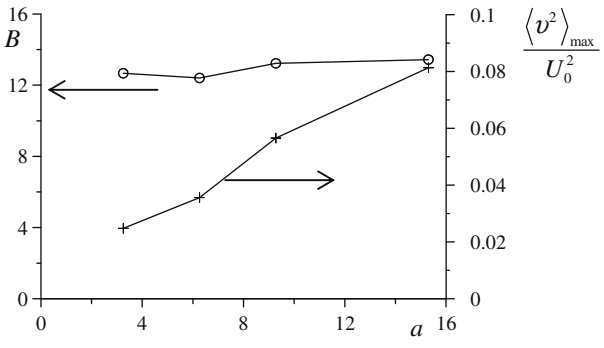

Fig. 21. Effect of forcing amplitude ($St = 0.52$) on the growth rate at $r/d = 0.61$ and maximum value at $z/d = 0.5$ of the radial component of TKE in a free jet at $S = 0.41$.

3.4. Forcing effect on jet with high swirl rate

This section reports the forcing effect on the swirling jet flow at a relatively high swirl rate, i.e., $S = 1.0$. For this flow regime, the recirculation zone, which in the present study was selected as evidence of the VB, was observed. Initial distributions of velocity fluctuations as well as the spatial distributions of the TKE components and instantaneous velocity fields are presented for the various forced conditions. It is important to note that, for the case of $S = 1.0$, the effect of forcing at $St = 0.52$ was less pronounced, while the forcing at $St = 1.2$ with amplitude a greater than 5% led to a significant change of the flow structure. Similar but more pronounced behavior was observed for the whole flow field and is discussed in Section 3.4.2.

3.4.1. Inflow distributions

Fig. 25 shows intensities of velocity fluctuations across the nozzle exit for the swirling jet at $S = 1.0$. As with the previous flow cases, distributions of w' and υ' were quite similar for the unforced case and most of the forced cases. However, the forcing at $St = 1.2$ led to different flow conditions depending on forcing amplitude. For the forcing amplitude greater than 5%, a significant difference in w' and υ' distributions appeared: values of υ' became lower, while w' was significantly greater than in the unforced case. The reason for the change in distributions is discussed in more detail below. For the case without forcing, the average values of u' and w' for $r/d < 0.4$ were found to be 35% and 39%, respectively. These values are significantly greater than those for the cases of $S = 0$ and 0.41. While forcing at $St = 0.52$, the average value of u' was found to increase in a way similar to the previous flow regimes. Again, w' and υ' were almost unchanged. However, when forcing at $St = 1.2$ was applied with $a > 5\%$ magnitude, u' and υ' decreased in some degree and w' increased. In this case, for both values of the amplitude tested, namely $a = 5.1\%$ and 6.9%, distributions of the intensities were

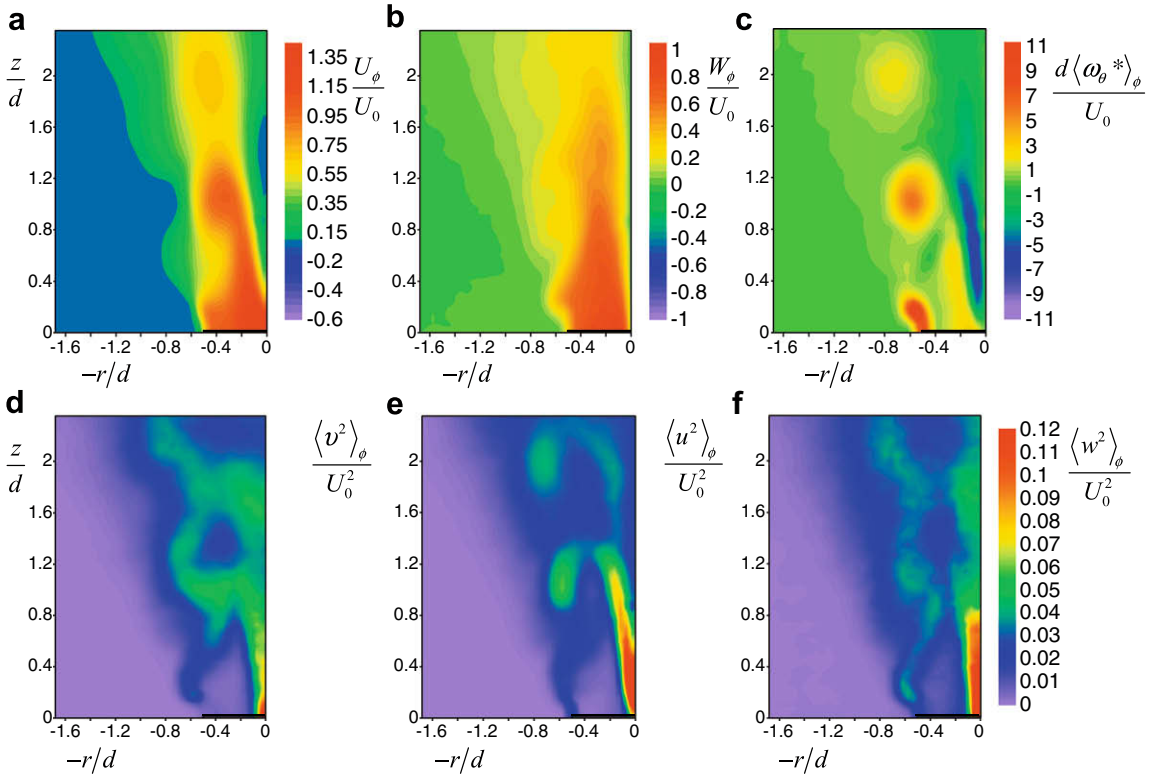

Fig. 22. Phase-averaged results for a forced free swirling jet at $S = 0.41$, $St = 0.52$; $a = 6.3\%$, $\phi = 0$.

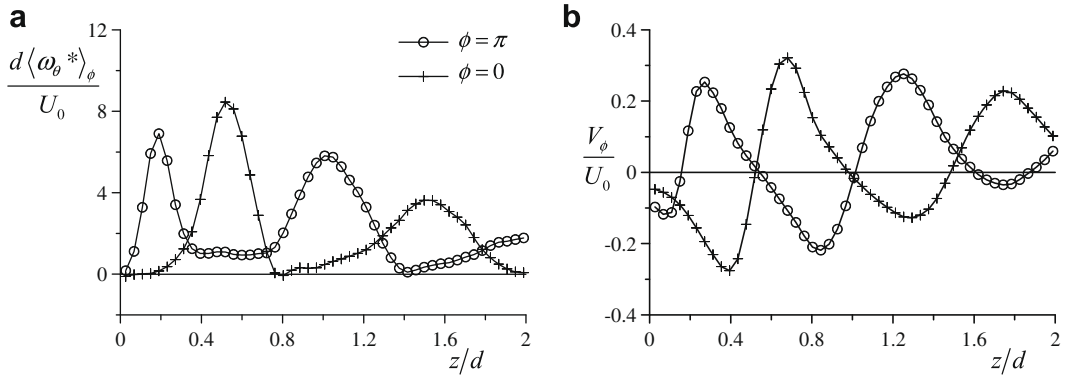

Fig. 23. Distributions of the phase-averaged (a) azimuthal vorticity and (b) radial velocity along the mixing layer $r/d = 0.61$ of a forced ($St = 0.52$, $a = 6.3\%$) swirling jet at $S = 0.41$.

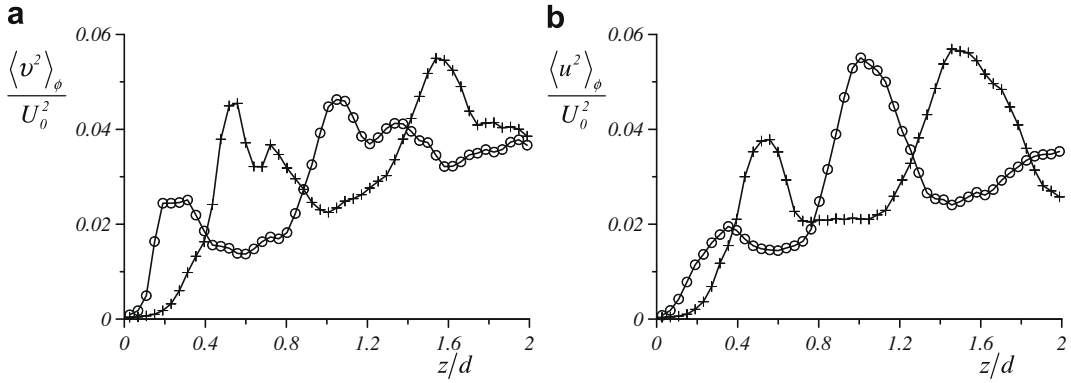

Fig. 24. Distributions of the phase-averaged (a) radial and (b) axial component of TKE along the mixing layer $r/d = 0.61$ of a forced ($St = 0.52$, $a = 6.3\%$) swirling jet at $S = 0.41$.

found to be nearly the same. It will be shown below that in these cases the forcing significantly affects the whole tested flow field, not only the vicinity of the nozzle.

3.4.2. Spatial distributions

Fig. 26 shows the spatial distributions of the TKE components for the most representative cases of the forced jet at $S = 1.0$. As with

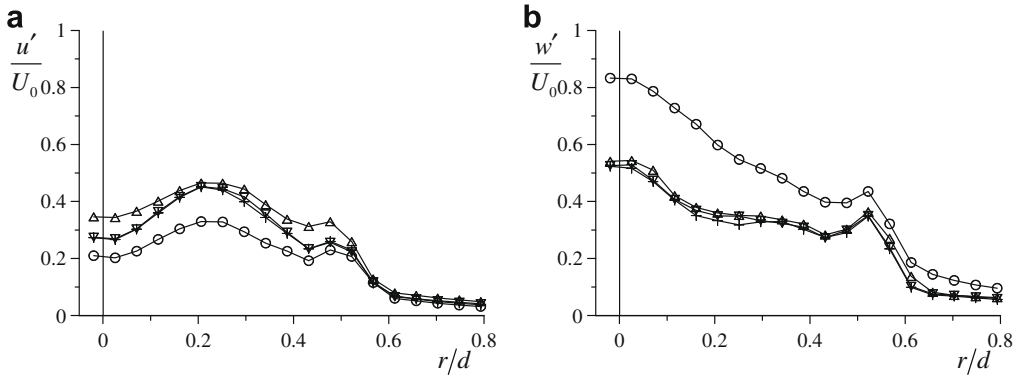

Fig. 25. Intensities of the (a) axial and (b) azimuthal velocity fluctuations near the nozzle exit ($z/d \approx 0.04$) for a swirling jet at $S = 1.0$. See Fig. 8 for the legend.

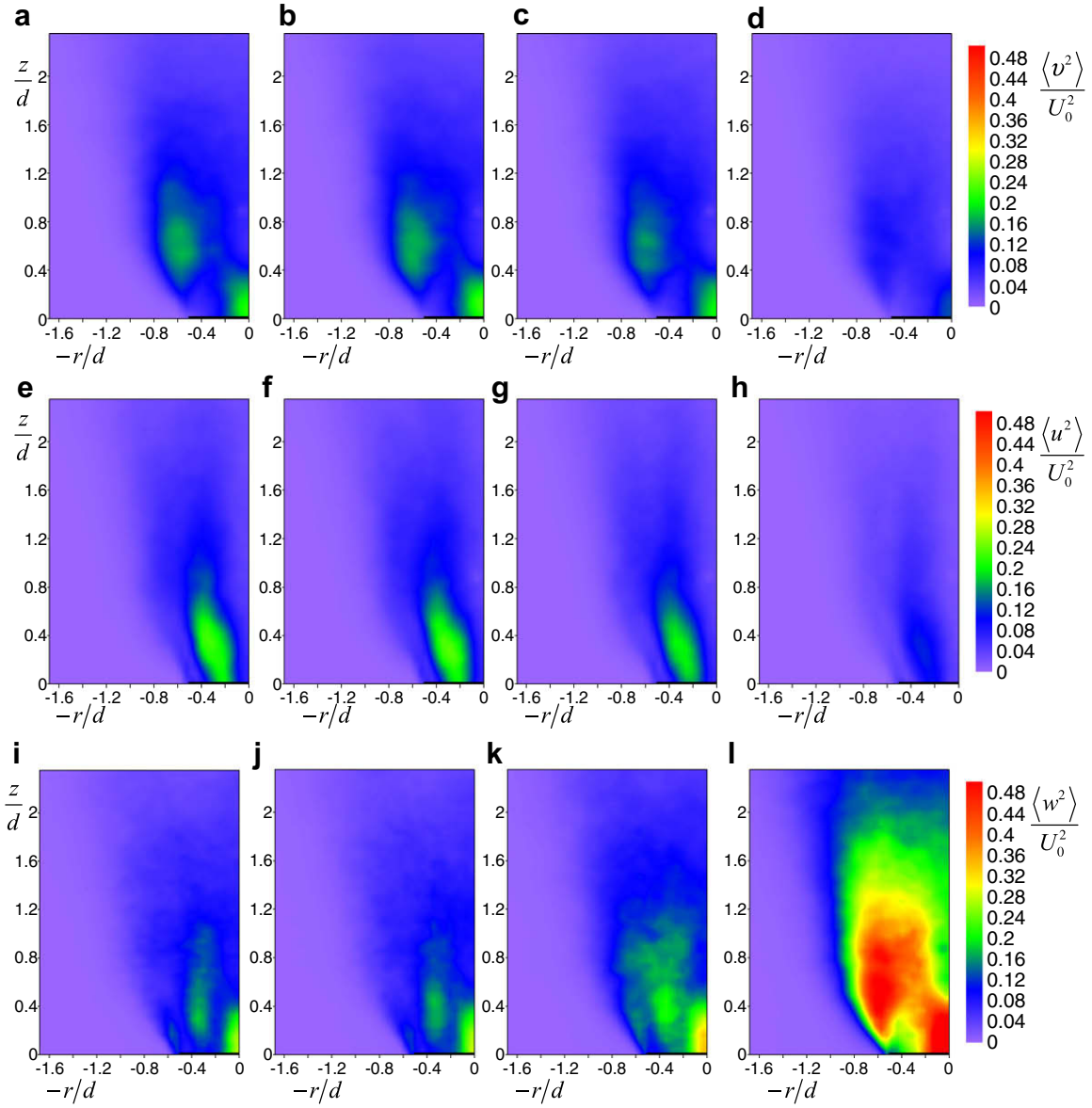

Fig. 26. Components of TKE for a free jet at $S = 1.0$. (a), (e), (i): $St = 0$; (b), (f), (j): $St = 0.52$, $a = 6.3\%$; (c), (g), (k): $St = 1.2$, $a = 4.2\%$; (d), (h), (l): $St = 1.2$, $a = 5.1\%$.

the effect on initial distributions described above, forcing at $St = 0.52$ did not lead to significant changes in magnitudes of TKE components (Fig. 26b, f and j) in the whole studied flow field, and only a moderate decrease of the longitudinal size of the recirculation zone was observed (not shown in the paper). Generally, for the unforced flow and for the case of $St = 0.52$, $\langle \upsilon^2 \rangle$ had the maximum of $0.23U_0^2$ in the mixing layer inside the recirculation zone, $\langle u^2 \rangle$ reached $0.21U_0^2$ and $0.17U_0^2$ at the jet axis and in the outer mixing layer, respectively. $\langle w^2 \rangle$ was observed to reach $0.25U_0^2$ and $0.17U_0^2$ at the jet axis and in the inner mixing layer, respectively. As was already mentioned, when the forcing was applied at $St = 1.2$ (which was found to correspond to a maximum of preliminary calculated one-dimensional spatial spectra), the effect on the TKE distributions was found to be substantial. For forcing amplitudes below 5%, $\langle w^2 \rangle$ grew in some degree, while $\langle u^2 \rangle$ and $\langle \upsilon^2 \rangle$ remained almost unchanged (cf. Fig. 26 a and c, e and g, i and k). When the amplitude value exceeded 5%, the flow pattern changed abruptly: $\langle u^2 \rangle$ and $\langle \upsilon^2 \rangle$ decreased with amplitude (the values of $\langle \upsilon^2 \rangle$ and $\langle u^2 \rangle$ became two times lower), while $\langle w^2 \rangle$ became greater (up to 0.7 of U_0^2), as did the total TKE (which increased by 1.4 times).

In order to validate such nontrivial behavior of the velocity components, which might appear as artifacts in Stereo-PIV measurements, the special calibration check was carried out. To ensure that there were no faults in stereo calibration (which could be caused, for example, by a facility vibration) during the experiment, the disparity maps were calculated for two cases: $St = 1.2$, $a = 4.2\%$ and $St = 1.2$, $a = 5.1\%$. It was found that there is no noticeable difference in calibration quality between these two cases, or between these cases and the unforced case, which was initially used for the estimation of the correction parameters for Stereo PIV.

To demonstrate the difference in vortical structure of the forced swirling jet, the spatial distributions of normalized instantaneous velocity and vorticity fields are presented in Fig. 27. The azimuthal

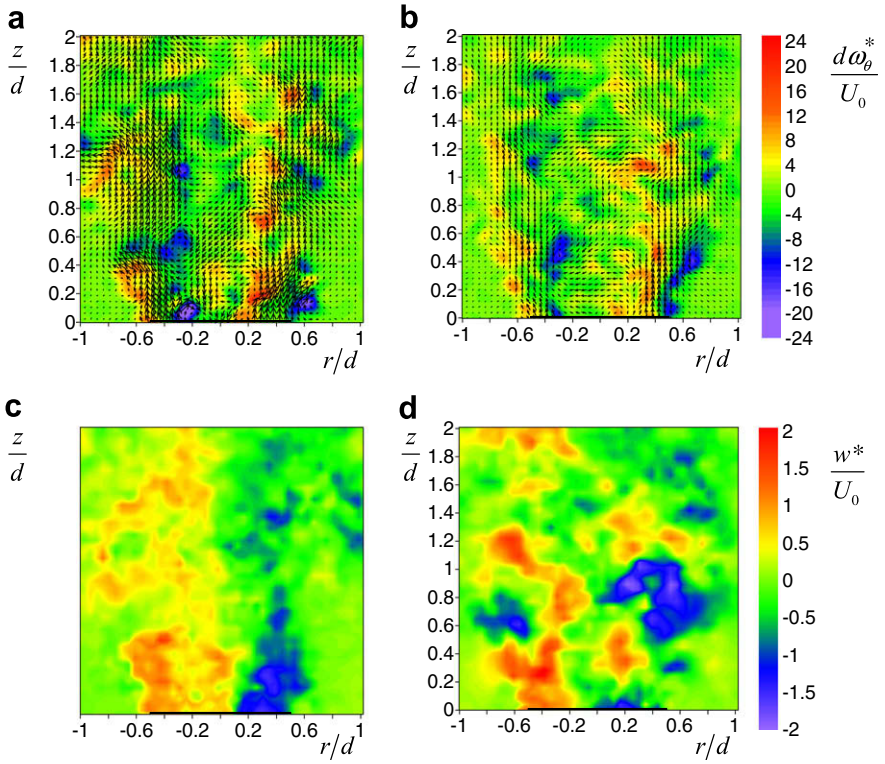

Fig. 27. Examples of instantaneous velocity and vorticity fields for free jet at $S = 1.0$. (a), (c) $St = 0.52$, $a = 15\%$; (b), (d) $St = 1.2$, $a = 5.1\%$. Azimuthal velocity distributions are shown in Figs. (c) and (d).

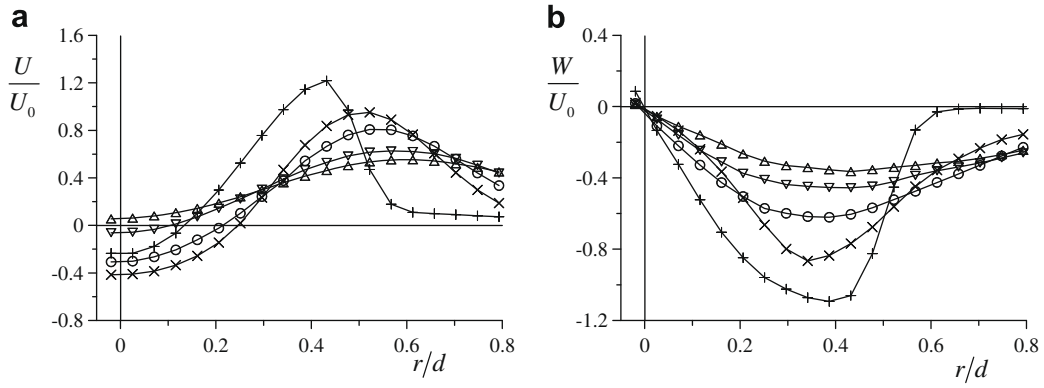

Fig. 28. Radial distributions of the (a) axial and (b) azimuthal mean velocity across an unforced free jet at $S = 1.0$. For the legend, see Fig. 29.

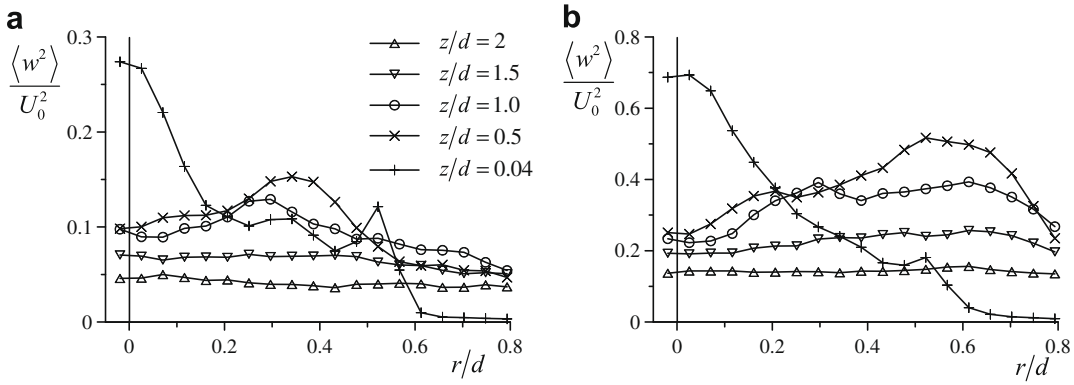

Fig. 29. Radial distributions of the azimuthal component of TKE across a free jet at $S = 1.0$. (a) Unforced jet, (b) $St = 1.2$, $a = 5.1\%$.

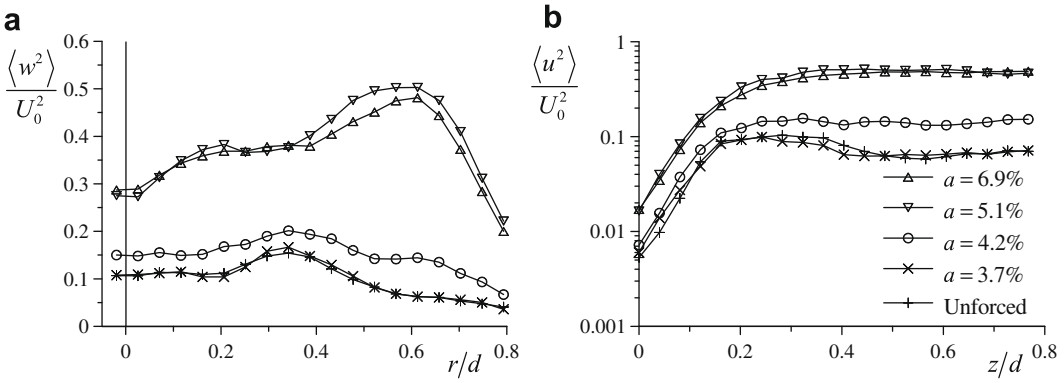

Fig. 30. Effect of forcing amplitude ($St = 1.2$) on the azimuthal component of TKE in a free jet at $S = 1.0$. (a) $z/d = 0.5$, (b) $r/d = 0.61$ cross-sections.

components of velocity (Fig. 27c and d) and vorticity are shown as scalar maps.

The reverse flow which was observed for the unforced flow was unaffected by the forcing. Comparing the unforced case and forcing at $St = 0.52$, no significant difference in the instantaneous jet structure was found. However, in the case of $St = 1.2$ with amplitude above 5%, the vortices were found to be less pronounced and to have a smaller size. More significant differences were observed in distributions of the instantaneous azimuthal velocity w^* plotted in Fig. 27c and d. While for the unforced jet and for $St = 0.52$, the azimuthal velocity was mainly positive to the left of the jet axis and negative to the right of the axis (in the coordinates used), large regions of w^* having opposite values were observed for the forced case at $St = 1.2$, $a > 5\%$. These regions were detected in most of the instantaneous velocity fields, attesting to the presence of the large-scale helical structures in the flow. These large-scale energy-containing structures must be the reason for high values of $\langle w^2 \rangle$ observed for the forced cases with $a \geqslant 5.1\%$, and thus are expected to be a key tool to increase turbulent mixing in highly swirling jets.

Evolution of the axial and azimuthal mean velocity distributions downstream is shown in Fig. 28. As with the case of $S = 0.41$, a greater spreading rate was observed for the swirling jet than for the $S = 0$ case. The distributions of the azimuthal and axial mean velocity are similar to the profiles for the case $S = 0.41$ (see Fig. 18), excepting the difference in magnitude of the profiles. The Sw calculated for the $z/d = 2$ cross-section was found to be 0.91.

Radial distributions of the azimuthal component of TKE for the various cross-sections are shown in Fig. 29. Flow regimes forced at $St = 1.2$ and $a = 5.1\%$ and unforced are compared. For both cases, $\langle w^2 \rangle$ has nearly uniform distribution in the radial direction for $z/d > 1$. The magnitude of $\langle w^2 \rangle$ was found to be $0.04U_0^2$ to $0.14U_0^2$ at the $z/d = 2$ cross-section for both the unforced and forced cases.

Fig. 30a presents radial distributions of $\langle w^2 \rangle$ at the $z/d = 0.5$ cross-section for the various forcing amplitudes at $St = 1.2$. For amplitudes below 5%, a maximum was observed at $r/d \approx 0.35$. For the unforced flow and for the case of $a = 3.7\%$, there was almost no difference in distributions, and increase of the $\langle w^2 \rangle$ magnitude was observed for $a = 4.2\%$. When the amplitude was 5.1% and 6.9%, the shape of the profiles changed (a local maximum appeared at $r/d \approx 0.6$) and the magnitude became significantly greater. This behavior is also reflected in Fig. 30b, which shows $\langle w^2 \rangle$ growth along the mixing layer ($r/d = 0.61$) for the various amplitudes of forcing at $St = 1.2$. As with the previous cases, $\langle w^2 \rangle$ was fit well by an exponential function in the initial region of the jet. One

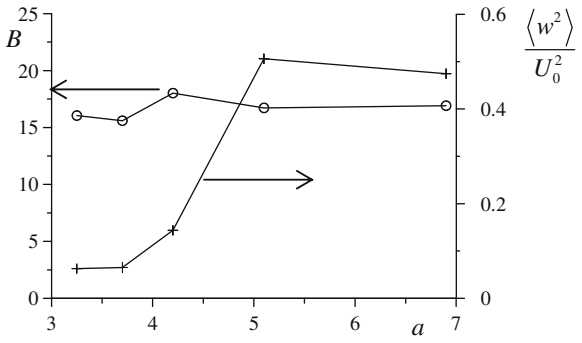

Fig. 31. Effect of forcing amplitude ($St = 1.2$) on the growth rate and value at $z/d = 0.5$ of the azimuthal component of TKE in a free jet at $S = 1.0$. $r/d = 0.61$ cross-section.

can clearly observe that the slope of $\langle w^2 \rangle$ in the initial region is nearly the same for all the amplitudes tested. The growth rate B is shown in Fig. 31 together with values of $\langle w^2 \rangle$ in the outer mixing layer at $r/d = 0.61$ and $z/d = 0.5$. For the different a, the growth rate was found to be around 16, which is the highest rate among the tested jet configurations. The values of $\langle w^2 \rangle$ presented in Fig. 31 demonstrate rapid growth with the amplitude. It was observed that for the amplitude from 5% to 7% there is no significant difference in the flow structure.

4. Conclusions

The present work presents experimental results of swirling jets at $Re = 8900$ and $S = 0-1.0$ obtained using a stereo PIV system. Generally, increase of the swirl rate S led to greater values of turbulent kinetic energy components in the initial region of the jets, and thus to a greater degree of turbulent mixing. For the swirling jet with clearly discernible vortex breakdown, the highest intensities of turbulent fluctuations were observed near the nozzle exit. The effect of external axisymmetric forcing of the swirling jets was studied in a wide range of forcing amplitudes. Two characteristic frequencies were used, $St = 0.52$ and 1.2, and the higher value was selected from preliminary analysis of the spatial one-dimensional spectra. It was shown that, for both the non-swirling jet and the jet with low swirl rate $S = 0.41$, forcing at $St = 0.52$ leads to an increased generation of turbulent kinetic energy with growth of forcing amplitude, and for $St = 1.2$, this effect is significantly less. Otherwise, for the jet at the high swirl rate $S = 1.0$, forcing at $St = 0.52$ had only a minor effect on the jet structure. The distinguishing behavior was revealed with forcing at $St = 1.2$. At relatively high amplitude ($u'_0 > 5\%$ of the mean flow rate velocity), an abrupt change in turbulent structure of the jet was observed: the total kinetic energy as well as its azimuthal component increased significantly. It was observed that large-scale structures rotating in the opposite direction to the mean flow are responsible for the mixing enhancement. Additional three-dimensional and/or time-resolved measurements with varying Re number, and forcing amplitude and frequency are necessary for clarification these structures appearing in the forced swirling jet with pronounced vortex breakdown. In summary, it can be concluded that combined application of external forcing and high swirl can be used as a tool for effective control of turbulent structure in jet flows.

Acknowledgements

This work is supported by RAS and SB RAS integration research projects and by the Russian Foundation for Basic Research, Grant No. 07-08-00213. The authors would like to thank Dr. S. Shtork for fruitful discussion.

References

Alekseenko, S.V., Markovich, D.M., Semenov, V.I., 1997. Effect of external disturbances on the impinging jet structure. In: Proceedings of the 4th World Conference on Experimental Heat Transfer, Fluid Mechanics and Thermodynamics, Brussels, Belgium, June 2–6, vol. 3, pp. 1815–1822.

Alekseenko, S.V., Kuibin, P.A., Okulov, V.L., Shtork, S.I., 1999. Helical vortices in swirl flow. J. Fluid Mech. 382, 195–243.

Alekseenko, S.V., Bilsky, A.V., Dulin, V.M., Markovich, D.M., 2007a. Experimental study of an impinging jet with different swirl rates. Int. J. Heat Fluid Flow 28, 1340–1359.

Alekseenko S.V., Bilsky A.V., Dulin V.M., Markovich D.M., 2007b, Experimental study of hydrodynamic structure of free and impinging turbulent jet using Stereo PIV. In: Proceedings of the 7th International Symposium on Particle Image Velocimetry, Rome, Italy, 11–14 September 2007, CD.

Alekseenko, S.V., Kuibin, P.A., Okulov, V.L., 2007c. Theory of Concentrated Vortices: An Introduction. Springer. p. 494.

Billant, P., Chomaz, J.-C., Huerre, P., 1998. Experimental study of vortex breakdown in swirling jets. J. Fluid Mech. 376, 183–219.

Broze, G., Hussain, F., 1996. Transitions to chaos in a forced jet: intermittency, tangent bifurcations and hysteresis. J. Fluid Mech. 311, 37–71.

Cala, C.E., Fernandes, E.C., Heitor, M.V., Shtork, S.I., 2005. Coherent structures in unsteady swirling jet flow. Exp. Fluid. doi:10.1007/s00348-005-0066-9.

Coudert, S.J.M., Schon, J.-P., 2001. Back-projection algorithm with misalignment corrections for 2D3C stereoscopic PIV. Meas. Sci. Technol. 12, 1371–1381.

Crow, S.C., Champagne, F.H., 1971. Orderly structure in jet turbulence. J. Fluid Mech. 48, 547–591.

Drobniak, S., Elsner, J.W., El-Kassem, E.-S.A., 1998. The relationship between coherent structures and heat transfer processes in the initial region of a round jet. Exp. Fluid 24, 225–237.

Dyban, E.P., Mazur, A.I., 1982. Convective heat transfer under conditions of jet flow past bodies. Kiev, Naukova Dumka, 303 (in Russian).

Duwig, C., Fuchs, L., 2007. Large eddy simulation of vortex breakdown/flame interaction. Phys. Fluid 19, 075103.

Foucaut, JM., Stanislas, M., 2002. Some considerations on the accuracy and frequency response of some derivative filters applied to particle image velocimetry vector fields. Meas. Sci. Technol. 13, 1058–1071.

Gallaire, F., Chomaz, J.-M., 2003. Mode selection in swirling jet experiments: a linear stability analysis. J. Fluid Mech. 494, 223–253.

Gallaire, F., Chomaz, J.-M., 2004. The role of boundary conditions in a simple model of incipient vortex breakdown. Phys. Fluid 16, 274–286.

Gallaire, F., Rott, S., Chomaz, J.-M., 2004. Experimental study of a free and forced swirling jet. Phys. Fluid 16, 1070–6631.

Gupta, A.K., Lilley, D.G., Syred, N., 1984. Swirl Flows. Abacus Press, Kent Engl.

Heinz, O., Ilyushin, B., Markovich, D., 2004. Application of a PDF based method for the experimental statistical processing of experimental data. Int. J. Heat Fluid Flow 25, 864–874.

Hussain, A.K.M.F., Zaman, K.M.B.Q., 1981. The 'preferred mode' of the axisymmetric jet. J. Fluid Mech. 110, 39–71.

Khalil, S., Hourigan, K., Thompsonc, M.C., 2006. Response of unconfined vortex breakdown to axial pulsing. Phys. Fluid 18, 038102.

Liang, H., Maxworthy, T., 2005. An experimental investigation of swirling jets. J. Fluid Mech. 525, 115–159.

Loiseleux, T., Chomaz, J.M., Huerre, P., 1998. The effect of swirl on jets and wakes: linear instability of the Rankine vortex with axial flow. Phys. Fluids 10, 1120–1134.

Loiseleux, T., Chomaz, J.M., 2003. Breaking of rotational symmetry in a swirling jet experiment. Phys. Fluid 15, 511–523.

Mehta, R.D., Wood, D.H., Clausen, P.D., 1991. Some effects of swirl on turbulent mixing layer development. Phys. Fluid A 3, 2716–2724.

Mourtazin, D., Cohen, J., 2007. The effect of buoyancy on vortex breakdown in a swirling jet. J. Fluid Mech. 571, 177–189.

Panda, J., McLaughlin, D.K., 1994. Experiments on the instabilities of a swirling jet. Phys. Fluid 6, 263–276.

Raffel, M., Willert, C., Kompenhans, J., Werely, S., 2007. Particle Image Velocimetry A Practical Guide, second ed. Springer, Berlin.

Ribeiro, M.M., Whitelaw, J.H., 1980. Coaxial jets with and without swirl. J. Fluid Mech. 96, 769–795.

Ruith, M.R., Chen, P., Meiburg, E., Maxworthy, T., 2003. Three-dimensional vortex breakdown in swirling jets and wakes: direct numerical simulation. J. Fluid Mech. 486, 331–378.

Scarano, F., David, L., Bsibsi, M., Calluaud, D., 2005. S-PIV comparative assessment: image dewarping + misalignment correction and pinhole + geometric back projection. Meas. Sci. Technol. 39, 257–266.

Shtern, V., Hussain, F., 1996. Hysteresis in swirling jets. J. Fluid Mech. 309, 1–44.

Stanislas, M., Okamoto, K., Kahler, C.J., 2005. Main results of the second international PIV challenge. Exp. Fluid. 39, 170–191.

Stanislas, M., Okamoto, K., Kahler, C.J., Westerweel, J., Scarano, F., 2008. Main results of the third international PIV challenge. Exp. Fluid. 45, 27–71.

Sun, D.-J., Hu, G.-H., Gao, Z., Yin, X.-Y., 2002. Stability and temporal evolution of a swirling jet with centrifugally unstable azimuthal velocity. Phys. Fluid. 14, 4081–4084.

Van Slooten, P.R., Pope, S.B., 1999. Application of PDF modeling to swirling and nonswirling turbulent jets. Flow Turbul. Combust. 62, 295–333.

Vejrazka, J., Tihon, J., Marty, Ph., Sobolik, V., 2005. Effect of an external excitation on the flow structure in a circular impinging jet. Phys. Fluid 17, 105102.1–105102.14.

Westerweel, J., 1994. Efficient detection of spurious vectors in particle image velocimetry data. Exp. Fluid 16, 236–247.

Westerweel, J., Scarano, F., 2005. Universal outlier detection for PIV data. Exp. Fluid 39, 1096–1100.

Zaman, K.B.M.Q., Hussain, A.K.M.F., 1981. Turbulence suppression in free shear flows by controlled excitation. J. Fluid Mech. 103, 133–159.